Pulmonary imaging with quantification of T1-relaxation and oxygen enhanced MRI

Kindvall, Simon

2018

[Link to publication](#)

Total number of authors:
1

Creative Commons License:
CC BY

Pulmonary imaging with quantification of T_1-relaxation and oxygen enhanced MRI

SIMON KINDVALL
DEPARTMENT OF MEDICAL RADIATION PHYSICS | LUND UNIVERSITY

Pulmonary imaging with quantification of T_1-relaxation and oxygen enhanced MRI

Simon Kindvall

LUND
UNIVERSITY

DOCTORAL DISSERTATION
by due permission of the Faculty of Medicine, Lund University, Sweden.
To be defended at Agardhsalen, CRC Malmö, 2018-12-14 at 13:00

Faculty opponent
Prof. Yannick Crémillieux, University of Bordeaux

Organization LUND UNIVERSITY	Document name DOCTORAL DISSERTATION
	Date of issue: 2018-12-14
Author: Simon Kindvall	Sponsoring organization

Pulmonary imaging with quantification of T_1-relaxation and oxygen enhanced MRI

Chronic obstructive pulmonary disease (COPD) is the third leading cause of death world-wide and is expected to take a progressively greater toll of lives as the population of the world ages. Apart from smoking cessation and decreased air-pollution there are few ways to stop this progressive, impeding and lethal condition. In order to combat lung disease in general and COPD in particular, there is a need for effective imaging biomarkers that can detect early pathologic changes in lung function, as well as detecting regional improvements after treatments and interventions.

Quantification of the longitudinal relaxation time (T_1) in the lung has been suggested as an imaging biomarker for several types of lung diseases, moreover, the addition of oxygen gas as a paramagnetic contrast agent (oxygen enhanced, OE-MRI) has been suggested to yield an imaging biomarker for the diffusing capacity of the lung.

The purpose of this thesis has been to evaluate both T_1-quantification and OE-MRI as imaging biomarkers for lung function in healthy volunteers and review previous models of these imaging biomarkers for lung disease.

A group of 35 healthy volunteers were recruited to perform pulmonary imaging with T_1-quantification and OE-MRI as well as pulmonary function tests. Stepwise linear regression of all pulmonary function parameters revealed that T_1 varied with lung volume, but was best described as a function of age and sex in the whole subject group. This finding is accompanied with physiological description of T_1 as a function of blood T_1 and blood volume, where hematocrit and residual volume vary with age and sex.

The diffusing capacity of the lung for carbon monoxide ($D_{L,CO}$) was also measured in the cohort and compared to the change in longitudinal relaxation rate after breathing oxygen (ΔR_1). The previously described correaltion between $D_{L,CO}$ and ΔR_1 could not be detected in the healthy subject group. Instead, a model including age, sex and BMI proved to yield the best fit to the data. This was interpreted as an influence of pulmonary shunt on ΔR_1 which increases with age and abdominal adiposity. Indeed, most pulmonary diseases studied with OE-MRI cause some degree of pulmonary shunt which is reflected in the lower ΔR_1.

A sub-group of the original cohort was recruited to perform airspace dimension assesment with nano-particles (AiDA) which is known to detect enlarged airspaces in COPD. The equilibrium signal, M0, which is calculated as a part of the T_1-quantification, was used to generate quantitative measures of airspace density which correlated with the airspace radius by AiDA.

Finally, two groups of volunteers (16 +12) were recruited to perform T_1 and ΔR_1 quantification with both gradient- and spin-echo sequences. In both groups the mean T_1 and ΔR_1 were different when quantified with gradient-echo compared to spin-echo. However, the gradient-echo measurements in both groups yielded very similar group means.

In conclusion, OE-MRI and T_1-quantification potentially provide imaging biomarkers for pulmonary shunt and blood volume, moreover, an imaging biomarker for lung density is available from the quantification protocol. These biomarkers exhibit variations with age, sex and BMI and may vary considerably with different quantification protocols.

Key words: Magnetic resonance imaging, diffusing capacity of the lung, oxygen enhanced MRI, pulmonary imaging, chronic obstructive pulmonary disease, sex-factors, age-factors, spirometry, oxygen, molecular oxygen paramagnetism

Classification system and/or index terms (if any)

Supplementary bibliographical information	Language: English

ISSN and key title: ISSN 1652-8220 Lund University, Faculty of Medicine Doctoral Dissertation Series 2018:152	ISBN 978-91-7619-721-9

Recipient's notes	Number of pages 90	Price
	Security classification	

Signature _Simon Kindvall_   Date 2018-11-08

Pulmonary imaging with quantification of T_1-relaxation and oxygen enhanced MRI

Simon Kindvall

LUND UNIVERSITY

Faculty of Medicine

Department of Medical Radiation Physics

Till Mamma, Pappa och mina Systrar

In my life I have found two things of priceless worth: learning and loving.
Nothing else – not fame, not power, not achievement for its own sake –
can possibly have the same lasting value.
Arthur C. Clarke, Rama Revealed

Table of Contents

Abbreviations

AiDA	Airspace dimension assessment with nanoparticles
CF	Cystic Fibrosis
COPD	Chronic obstructive pulmonary disease
CO-Hb	Carboxy-hemoglobin
Deoxy-Hb	Deoxygenated hemoglobin
$D_{L,CO}$	Diffusing capacity of the lung for carbon monoxide
ERV	Expiratory reserve volume
EVF	Erythrocyte volume fraction
FEV_1	Forced expiratory volume in 1 second
FLASH	Fast low angle shot (gradient echo)
FRC	Functional residual capacity
GINA	Global initiative for asthma
GOLD	Global Initiative for Chronic Obstructive Lung Disease
Hb	Hemoglobin
Hct	Hematocrit
HASTE	Half-Fourier Acquisition Single-shot Turbo spin Echo
HPV	Hypoxic Pulmonary Vasoconstriction
IC	Inspiratory capacity
IR	Inversion recovery
MRI	Magnetic resonance imaging
PFT	Pulmonary function test
Q	Perfusion or blood volume
R_1	Longitudinal relaxation rate ($R_1 = 1/T_1$)

R_2	Transverse relaxation rate ($R_2 = 1/T_2$)
r_1	Longitudinal relaxivity of contrast agent
RBC	Red blood cell
ROI	Region of interest
RV	Residual volume
SNR	Signal to noise ratio
T_1	Longitudinal relaxation time
T_2	Transverse relaxation time
TI	Inversion time
TLC	Total lung capacity
TSE	Turbo spin echo
UTE	Ultra-short echo time
V	Ventilation
VC	Vital capacity
WHO	World Health Organization

List of original papers

This thesis is based on the following four original papers, referred to as **Paper 1-4**.

1. Influence of age and sex on the longitudinal relaxation time, T_1, of the lung in healthy never-smokers

    Simon Kindvall, Sandra Diaz, Jonas Svensson, Per Wollmer, Dariuzs Slusarczyk , Lars E Olsson. *Journal of Magnetic Resonance Imaging*. 2016;43: 1250–1257. doi:10.1002/jmri.25085

2. The change of longitudinal relaxation rate in oxygen enhanced pulmonary MRI depends on age and BMI but not diffusing capacity of carbon monoxide in healthy never-smokers

    Simon Kindvall, Sandra Diaz, Jonas Svensson,Per Wollmer ,Lars E Olsson. *PLoS One*. 2017;12: e0177670.

3. Airspace Dimension Assessment with nanoparticles reflects lung density as quantified by MRI

    Laura Aaltonen, **Simon Kindvall,** Jonas Jakobsson, Jakob Löndahl, Lars E Olsson, Sandra Diaz, Sophia Zackrisson, Per Wollmer. *International Journal of Nanomedicine*. 2018;13: 2989–2995. doi:10.2147/IJN.S160331

4. The change in longitudinal relaxation rate in oxygen enhanced pulmonary MRI: inversion recovery HASTE versus Snapshot FLASH

    Simon Kindvall, Lars E Olsson. *Unpublished manuscript* 2018.

Abstract

Chronic obstructive pulmonary disease (COPD) is the third leading cause of death world-wide and is expected to take a progressively greater toll of lives as the population of the world ages. Apart from smoking cessation and decreased air-pollution there are few ways to stop this progressive, impeding and lethal condition. In order to combat lung disease in general and COPD in particular, there is a need for effective imaging biomarkers that can detect early pathologic changes in lung function, as well as detecting regional improvements after treatments and interventions.

Quantification of the longitudinal relaxation time (T_1) in the lung has been suggested as an imaging biomarker for several types of lung diseases, moreover, the addition of oxygen gas as a paramagnetic contrast agent (oxygen enhanced, OE-MRI) has been suggested to yield an imaging biomarker for the diffusing capacity of the lung.

The purpose of this thesis has been to evaluate both T_1-quantification and OE-MRI as imaging biomarkers for lung function in healthy volunteers and review previous models of these imaging biomarkers for lung disease.

A group of 35 healthy volunteers were recruited to perform pulmonary imaging with T_1-quantification and OE-MRI as well as pulmonary function tests. Stepwise linear regression of all pulmonary function parameters revealed that T_1 varied with lung volume, but was best described as a function of age and sex in the whole subject group. This finding is accompanied with physiological description of T_1 as a function of blood T_1 and blood volume, where hematocrit and residual volume varies with age and sex.

The diffusing capacity of the lung for carbon monoxide ($D_{L,CO}$) was also measured in the cohort and compared to the change in longitudinal relaxation rate after breathing oxygen (ΔR_1). The previously described correlation between $D_{L,CO}$ and ΔR_1 could not be detected in the healthy subject group. Instead, a model including age, sex and BMI proved to yield the best fit to the data. This was interpreted as an influence of pulmonary shunt on ΔR_1 which increases with age and abdominal adiposity. Indeed, most pulmonary diseases studied with OE-MRI cause some degree of pulmonary shunt which is reflected in the lower ΔR_1.

A sub-group of the original cohort was recruited to perform airspace dimension assesment with nano-particles (AiDA) which is known to detect enlarged airspaces in COPD. The mean equilibrium signal, M_0, which is calculated as a part of the T_1-

quantification, was used to generate quantitative measures of airspace density which correlated with the airspace radius by AiDA.

Finally, two groups of volunteers (16 +12) were recruited to perform T_1 and ΔR_1 quantification with both gradient- and spin-echo sequences. In both groups the mean T_1 and ΔR_1 were different when quantified with gradient-echo compared to spin-echo. However, the gradient-echo measurements in both groups yielded very similar group means.

In conclusion, OE-MRI and T_1-quantification potentially provide imaging biomarkers for pulmonary shunt and blood volume, moreover, an imaging biomarker for lung density is available from the quantification protocol. These biomarkers exhibit variations with age, sex and BMI and may vary considerably with different quantification protocols.

Populärvetenskaplig sammanfattning

Bildtagning med magnetresonans (mangetic resonance imaging eller MRI) är en fascinerande teknik som använder magnetfält och radiovågor för att skapa detaljerade bilder av kroppens innanmäte. Tvärt om mot vad många tror så finns det ingen "magnetröntgen" i MR-kameran, och därmed ingen skadlig joniserande strålning. Detta gör det möjligt att utföra upprepade undersökningar på friska och sjuka försökspersoner utan att undersökningen själv skadar kroppen. Samtidigt skryter MRI med sjukvårdens kanske mest informationsrika bilder.

Tyvärr är MR oerhört dåligt för att studera just lungor. Lungorna innehåller vanligtvis mest luft, vilket från början inte ger någon MR-signal. Som om det inte räcker är MRI oerhört långsamt och ingen kan hålla andan så länge som det krävs för att ta riktigt bra MR-bilder. Trots detta finns fantastiska möjligheter med bildmarkörer för sjukdomstillstånd som enkelt kan fångas på MR-kameran. Två sådana bildmarkörer är T_1-relaxationstid och syreförstärkning.

T_1-relaxationstid är en av de tre grundläggande vävnadsparametrarna i MRI, bredvid T_2 och protontäthet (PD). Dessa kan jämföras med grundfärgerna rött, grönt och blått, där alla MR-bilder i grunden består av olika T_1, T_2 och PD. I tidigare mätningar har man sett att T_1 varierar mycket mellan friska och sjuka lungor, speciellt har man sett att kronisk obstruktiv lungsjukdom (KOL) förkortar T_1, likaså fibros och till viss del rökning. Enligt en tidigare rapport hade en person som rökt länge kortare T_1, men är det för att denne rökt länge, eller bara levt länge? I den första delen av denna avhandling kvantifierades därför T_1 i en grupp friska frivilliga icke-rökare för att undersöka om det fanns något åldersberoende för T_1. Resultatet presenterades på en internationell konferens och fick åhörarna att bokstavligt talat tappa hakan. Vi kunde påvisa en stark köns- och ålderskorrelation, där unga kvinnor har en mycket längre T_1 än både män och äldre kvinnor. Tolkningen av resultatet får oss att tro att T_1 egentligen är en bildmarkör för blodvolym, då blod har lång T_1 och de flesta sjukdomstillstånd – samt hög ålder – leder till lägre blodvolym i lungan.

Syreförstärkt MR är också baserat på T_1-kvantifiering, men går ut på att mätningar görs både innan och under det att försökspersonen andas ren syrgas i några minuter. Syre är helt ofarligt att andas i flera timmar, så några minuter är verkligen helt riskfritt. Syre får T_1-relaxationstiden i lungan att bli kortare och signalen i bilden att förstärkas – därav syreförstärkt MR. Tidiga mätningar antydde att syreförstärkt MR kunde mäta

lungans diffusionskapacitet, hur effektivt syrgas tas upp av lungan. Andra delen i denna avhandling mätte därför också syreförstärkningen i en grupp friska frivilliga, tillsammans med alla relevanta mått på lungfunktion. Även här förvånade resultatet många, även om det inte mottogs lika entusiastiskt som första gången: Det tidigare rapporterade sambandet mellan lungans diffusionskapacitet och syreförstärkningen fanns inte i de friska frivilliga. Istället fann vi en väldigt stark korrelation mellan syreförstärkning och kön, ålder och BMI. Detta resultat kunde också tolkas med en fysiologisk förståelse. I friska individer är faktiskt inte syreupptaget begränsat av diffusion, i stort sett allt blod blir fullt syresatt om det kommer i kontakt med frisk luft. Problem uppkommer om en del av lungan inte får tillgång till luft, och blod passerar utan att bli syresatt. Detta är precis vad som händer vid hög ålder eller då fett i buken trycker på lungan – delar av lungan stängs och förblir icke-syresatta.

Vidare visade vi att vår metod för att mäta T_1 också kan användas för att mäta protontäthet (en annan av de tre "grundfärgerna" i MRI). Protontäthet är kort sagt mängden vattenmolekyler i lungan, och minskar såklart vid svår lungsjukdom då vävnaden bryts ner (då all kroppens vävnad består av ca 70% vatten). I gruppen av friska frivilliga var alla mått på protontäthet korrelerade med den uppskattade radien på lungans alveoler (de minsta luftblåsorna i lungan där gasutbyte sker). Detta är väldigt viktig information vid KOL, eftersom ett kardinalsymptom är just nedbrytning av väggarna mellan alveolerna.

Slutsatserna från detta arbete är att en mätning med syreförstärkt MR av lungorna eventuellt kan ge information om blodmängd, syresättning och vävnadstäthet i lungan, genom de tre parametrarna T_1-relaxationstid, syreförstärkning och protontäthet, samt att dessa parametrar kan variera med åtminstone kön och ålder hos en frisk population. Eftersom det inte finns några kända skadliga effekter av undersökningen, är det möjligt att utforma studier på riskgrupper för lungsjukdom, eller på patienter som testar nya behandlingar, med flera uppföljande mätningar. Förhoppningsvis uppmuntrar denna avhandling också fler till att göra tvärvetenskapliga projekt då vi tydligt visat hur både fysiologi och fysik är nödvändigt för att tolka resultaten från samtliga delarbeten.

1 Introduction

Before doing anything that will probably cost you considerable effort and time (such as a four year full time PhD project) you want to ask yourself – Why?

When it comes to pulmonary imaging the question is easily answered by the World Health Organisation (WHO). As of 2016, COPD, lower respiratory infections and airway cancers together take an annual toll of 7.7 million deaths, with only ischemic heart disease being a larger burden at 9.4 million [1]. Chronic obstructive pulmonary disease (COPD) alone is the third largest cause of death (after cardio- and cerebrovascular disease); takes more than three million lives annually; and is predicted to become an even greater burden as the global population ages [2]. Moreover, there is evidence that in the future women will suffer more as they may be undertreated and be more susceptible to exacerbations [3].

In order to lift the global burden of lung disease, we cannot sit back and rely on smoking cessation and decreased air pollution. Instead we must also seek to understand all lung disease and detect it early, before it damages the lung irreversibly.

The functions of the lung can generally be reduced to three processes involving the transfer of oxygen and carbon dioxide [4]:

- Ventilation refers to transfer of gas between the mouth and the alveoli.

- Diffusion of gas is between the alveolar space and the pulmonary capillaries.

- Perfusion is the flow of blood that transfers gas to and from the lungs.

Integrity of lung functions is dependent on all three processes; however, the most common way to diagnose lung disease is spirometry – the simple measurement of lung volumes and expiratory flow (ventilation). For example, the diagnosis and classification of chronic obstructive pulmonary disease (COPD) is based on spirometry alone, apart from the presentation of relevant symptoms and previous inhalation of harmful agents [5].

Although several sophisticated imaging methods are available and widely used in the clinic, no single imaging modality reveals the true "functions" on the lung. X-ray based computerized tomography (CT) is fast, provides excellent morphological information, and can be used with an intravenous contrast agent to reveal disruption in pulmonary perfusion (emboli) [6]. However, CT provides no information about the ventilation or

diffusion of gas in the lung. Nuclear medicine imaging can also be used to study aspects of lung function, and the sequential inhalation and injection of radioactive tracers allows the calculation of a ventilation and perfusion image, which is highly informative, although still lacking the diffusion information. Moreover, although both CT and nuclear medicine imaging (SPECT and flat scintillation imaging) can be safely used in all populations, they should be used with caution and in limited number to reduce the dose of ionizing radiation.

Oxygen enhanced MRI of the lungs is based on the simple fact that inspired oxygen gas acts as a paramagnetic contrast agent and will increase the signal in a T_1 weighted MRI image [7]. Since no MRI signal arises from the air, there will only be a change in signal if the inspired oxygen reaches the pulmonary interstitial water or blood. Ideally, OE-MRI thus provides an opportunity to directly study integrated lung function – including the evasive diffusion component. However, as we will see in this dissertation, nothing is ever that simple.

The proposal to use OE-MRI to study pulmonary function came in 1996 [8] and it was later assumed that the signal change in OE-MRI reflects the diffusing capacity of the lung [9] or that OE-MRI is a way to measure pulmonary oxygen tension (P_{O2}) [10,11]. This is based on the assumption that oxygen acts as an inert contrast agent with a single value of the MRI relaxivity – meaning that the same change in oxygen tension will always give rise to the same change in relaxation rate [12]. By presenting results from OE-measurements in healthy individuals and reviewing available literature in OE-MRI and adjacent fields, this thesis presents evidence that a physiologic understanding of the OE-effect is necessary to interpret OE-measurements:

- Lung perfusion is highly dependent on oxygen tension and areas with low oxygen tension will be shut by precapillary pulmonary arterioles (hypoxic pulmonary vasoconstriction) [13]. Accordingly, inhalation of oxygen will potentially effect flow and blood volume in the lung [14,15].

- The relaxivity of gadolinium-based contrast agents have been proven to vary with macromolecule content [16,17] and the relaxivity of several different paramagnetic ions vary with the protein solution [18]. The molecular oxygen relaxivity has been shown to be higher in whole blood than in plasma or cerebrospinal fluid [19], supporting the notion that oxygen paramagnetic relaxivity is also dependent on protein concentration.

- The lung blood is partitioned in three basic compartments, non-oxygenated (pulmonary arterial) blood, capillary blood, and oxygenated (pulmonary venous) blood. The OE-effect as discussed hitherto is only relevant in the latter half of these compartments where the hemoglobin is fully saturated and oxygen tension can rise over 100 mmHg. Indeed, non-oxygenated hemoglobin (deoxy-Hb) has a considerable paramagnetic relaxation effect [20] and any

increase in oxygen saturation will lead to a *negative* OE-effect in the pulmonary arterial compartment.

For all these reasons we need a more holistic (physiological, physical and chemical) view of the pulmonary OE-effect, and remove ourselves from the naïve idea that oxygen gas can be treated as a simple paramagnetic contrast agent.

1.1 The aims of this thesis:

- Establish a normative reference for pulmonary OE and T_1-measurements in a healthy population with respect to age and sex **Paper 1 and 2**

- Give a plausible explanation for the variations of OE and T_1 in this normal population **Paper 1 and 2**

- Show that OE-measurements with the Look-Locker sequence provides additional imaging biomarkers relevant for lung disease **Paper 3**

- Show that differences in MRI methodology will affect both quantitative T_1 and oxygen enhancement. Specifically, spin-echo and gradient echo sequences may yield different mean values **Paper 4**

- Provide a summary of the state of the art in OE-MRI for anyone interested in implementing it.

2   Lung physiology for physicists

The function of the lung is to exchange gases with the environment to provide oxygen necessary for metabolism, expel carbon dioxide and regulate the acidity of the blood. The first thing that should be noted about the lung is that it normally operates at a very submaximal level. For example, when blood flows into the lung to get oxygenated, it is fully saturated after 1/3 of the time spent in the alveolar capillary. Moreover, while a regular effortless breath is usually 500 ml, the vital capacity (maximal size of a breath) is approximately 5 liters for a male and 4 liters for a female [21]. The lung thus has an enormous extra capacity for gas uptake, which is only nearly maximized during elite sporting events [22] and in all cases of normal physiology, oxygen transport in the body is not limited by diffusion or ventilation but by the cardiac pumping ability [4]. The unnerving implication of this is that an otherwise healthy person, who is affected by a progressive lung disease such as COPD, may lose 50% of their pulmonary function before being noticeably impaired by it in everyday non-aerobic activity and seeking medical care.

2.1   The lung consist of 30% blood

Since the function of the lung is to get gases in and out of the blood, the blood itself will be a central constituent of the lung. Indeed, the mean weight of male human lungs have been shown to be 445 g (SD 159g) for the right, 395 g (SD 147 g) for the left lung [23] and probably around 400 g for pulmonary blood [24]. This blood is partitioned roughly equally between the precapillary lung arteries, alveolar capillaries and postcapillary pulmonary veins [24]. This however, may be dramatically changed by hypoxia, or any endo- or exogenous signal molecule, which activates pre- or post-capillary vasoconstriction. Specifically, hypoxia activates small artery vasoconstriction and decrease capillary pressure; whereas histamine or noradrenaline activate venular vasoconstriction and thus increase capillary pressure [13].

2.2   Elastic recoil keeps airways open

An important concept in lung physiology is the elastic recoil of lung tissue (force/distention), which tells us that a positive airway pressure – or a negative transpulmonary pressure – is needed to inflate the lung. Often, the same property is described with the *compliance* of the lung which is basically the inverse of the elastic recoil. A normal lung expands by being pulled out by the rib cage and diaphragm through muscular effort (negative transpulmonary pressure), whereas the expulsion of air depends on the lung tissue's innate ability to recoil. During natural aging and in COPD the lung loses some of its elastic recoil properties and the expulsion of air becomes limited [25,26]. Moreover, the small airways, from the bronchiolar level, do not contain cartilage rings to keep them open but rely on elastic recoil to be pulled open. Since the elastic recoil depends on lung volume, the elastic recoil will decrease while exhaling until it is insufficient to keep the airways open and the lung will close – trapping the remaining air inside. The lung volume at which this air-trapping and airway closure occurs is defined as the residual volume (RV). According to the previous discussion residual volume will increase with age, i.e. the lung will close at a higher volume [27].
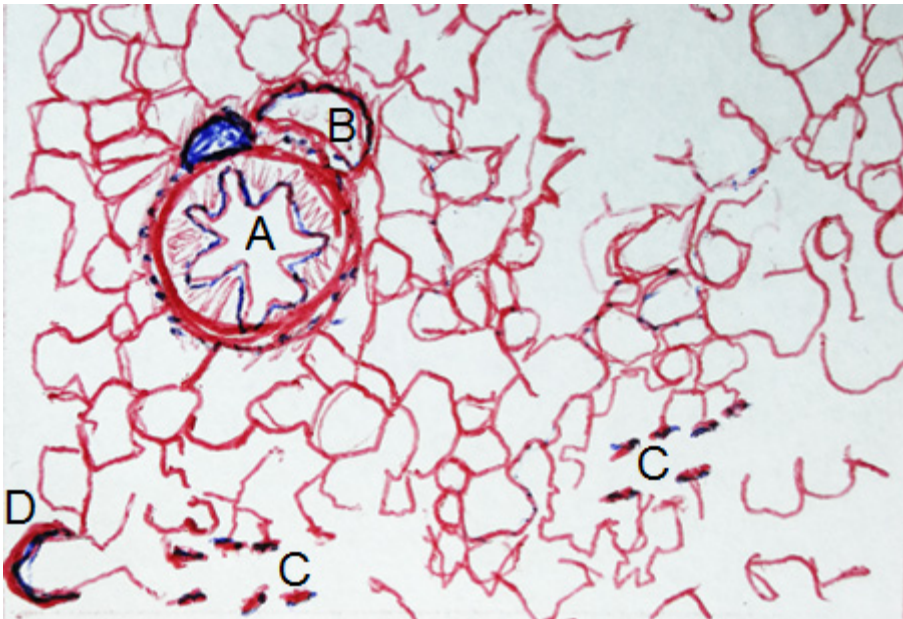
Figure 1 Sketch of a hematoxylin eosin-stained lung slice from [28]. The bronchiole with its muscular wall (A) is very prominent, along with a venule (B) and lymph node. There are also alveolar ducts (C) and a terminal bronchiole (D). The white is all airspace and the thin walls are the alveolar walls with capillaries. It is easy to appreciate that if the lung tissue is compressed, the airways will also compress, limiting airflow. It is also easy to appreciate that a substantial fraction of the lung weight is blood.
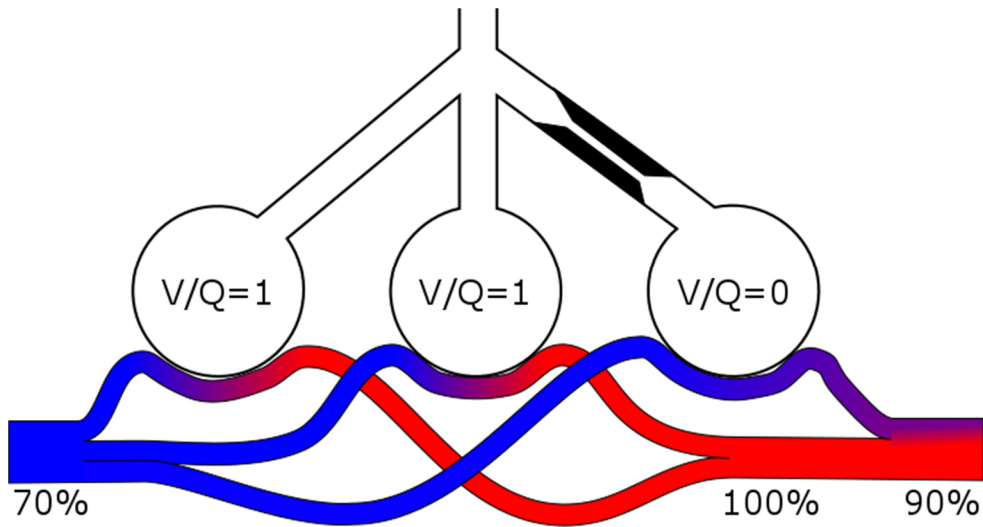
Figure 2 Schematic drawing of pulmonary shunt after a V/Q inequality. Percentages indicate oxygen saturation. Three alveoli are supplied by three capillaries. Although two gas exchange units work perfectly the final oxygen tension is severely reduced due to venous admixture. In healthy lungs, the vessels supplying the poorly ventilated area will shut due to Hypoxic Pulmonary Vasoconstriction.

2.3 Pulmonary shunt dramatically reduces arterial oxygen concentration

For the lung to function optimally the ventilation and perfusion, commonly notated as *V and Q,* must be matched – this means that any given region of the lung is both perfused with blood and ventilated during breathing. If a region of the lung is perfused but not ventilated – because of airway collapse, mucus plugs, or airway constriction – any blood passing through will remain non-oxygenated and lower the efferent oxygen concentration of the whole system (Figure 2). This *venous admixture* or *shunting* will result in a dramatically lower arterial oxygen concentration in an otherwise healthy lung, especially in the senile lung [29]. Importantly, in obese individuals abdominal fat forces the lung to operate very close to the RV [30,31]. Since RV is the definition of airway closure, obese individuals will have increased venous admixture and lower arterial oxygenation [32,33].

2.4 Hypoxic pulmonary vasoconstriction prevents shunt

The lung actively counteracts V/Q inequality and shunt by *hypoxic pulmonary vasoconstriction* (HPV). Hypoxia in the airspace mediate a slow (minutes) constriction of upstream small pulmonary arteries, which is rapidly (seconds) reversed when oxygen concentration rise [13]. Chronic HPV also cause hypertrophy of small arteriole muscle [34]. It is important to note that HPV increase the total resistance of the pulmonary circulation and consequently increase the pulmonary arterial pressure [35]. It is also noteworthy that HPV can be overridden by inflammation, which will cause a vasodilation even in non-oxygenated areas of the lung [36].

2.5 PFT and lung volumes

The most common measures of lung function is the combined measurement of FEV_1 (forced expiratory volume in one second) and FVC (the forced vital capacity). To measure FEV_1 and FVC a subject is told to inhale as much air as they possibly can and then exhale as forcefully and quickly as possible into an air-flow meter, until no more air can be further expelled. Since airway resistance depends on the elastic recoil of lung tissue as well as mucus and muscular tension in the airways, this simple test may reveal inflammatory, allergic and degenerative changes. In healthy subjects the FVC is the same as the vital capacity (VC), but in some lung disease the FVC will be smaller than the VC due to dynamic airway compression [37–39]. Using these volumes it is possible to differentiate between restrictive disease, in which the VC is restricted, and obstructive disease as anything limiting the quotient FEV_1/VC.

Other important lung volumes can be seen in figure 3. It should be noted that IC, VC and tidal volume can be measured with simple equipment, whereas RV, FRC and TLC requires some gas dilution technique or a body plethysmograph [4].
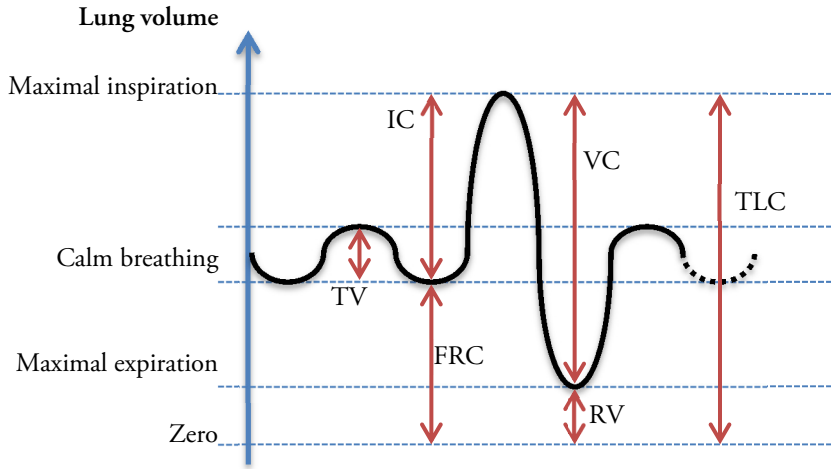
Figure 3 Tidal volume (TV) is the size of a regular calm breath; functional residual capacity (FRC) is the volume of air left after an effortless exhalation; inspiratory capacity (IC) is the maximum volume you can inhale after an effortless exhalation; residual volume (RV) is the volume of air trapped in the lung after maximal exhalation; vital capacity (VC) is the maximum amount of air that can be expelled after a maximal inhalation; and total lung capacity (TLC) is both IC+FRC or VC+RV.

2.6   Diffusing capacity of the lung

Diffusing capacity of the lung is a measure of the lungs ability to extract gas from the alveoli and depends on the diffusion of gas molecules across the alveolar membrane. Although the diffusion of oxygen is more interesting, it is more common and practical to measure the diffusing capacity of the lung for carbon monoxide ($D_{L,CO}$). The test for $D_{L,CO}$ involves the breathing of a small amount (0.3 %) of CO which, due to the very low driving pressure difference between alveolar air and blood, will equilibrate very slowly with the blood. However, as soon as the CO-molecule reaches the lung blood, it is rapidly and irreversibly absorbed by hemoglobin. These parameters – the low driving pressure and the rapid capture by Hb – make the transport of CO into the blood completely limited by diffusion and the available capillary blood volume. The diffusing capacity can be regarded as a flow across a membrane resistance and expressed as $D_{L,CO}^{-1} = D_m^{-1} + (\theta Q_c)^{-1}$ where D_m is the membrane diffusing capacity and Q_c is the capillary blood volume – thus $D_{L,CO}$ depends on membrane area and thickness as well as the available pulmonary blood volume [40]. Another way to express the diffusing capacity is the k_{CO} which is the $D_{L,CO}$ adjusted for alveolar volume: $D_{L,CO} = k_{CO}V_A$ which can be useful since people with large lungs will have large $D_{L,CO}$ [41].
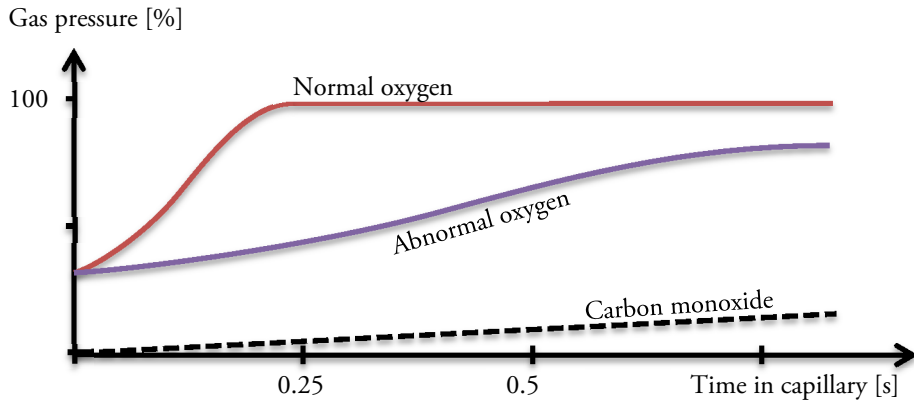
Figure 4 Gas transfer as a function of pulmonary capillary time for normal oxygen, abnormal oxygen and CO-transfer. Capillary oxygen is usually in equilibrium with alveolar oxygen after 0.25 s. At very high cardiac output – such as during Olympic sprinting – blood spends only 0.25 seconds in the capillary and gas transfer may be diffusion limited. Carbon monoxide diffuses way more slowly and CO-transfer is always diffusion limited **[4]**.

2.7 AiDA

Airspace dimension assessment with nanoparticles (AiDA) is a recently developed technique to assess the free diffusion paths in the distal airways [42,43]. It was used in **paper 3** of this thesis and thus requires some closer explanation. In very general terms, the subject inhales an aerosol of nanoparticles, holds the breath and exhales after 5-10 seconds. Due to the minuscule size of the nanoparticles they will move primarily by free diffusion in the distal airways. Consequently, the chance of adsorbing to the alveolar wall will depend on the time spent in the distal airway and the size of the alveoli. In a subject with the diffusion distance will be long and the particles will have a low chance of randomly hitting an alveolar wall and being adsorbed; conversely, in a subject with healthy lungs with a very fine microstructure the nanoparticles will have a large chance of adsorbing.

In the practical setting a subject will perform several inhalations with different breath-hold times. By controlling the inhaled and exhaled air volumes, as well as the nanoparticle concentration in the inhaled and exhaled air samples, the amount of nanoparticles deposited is easily calculated. The deposition will then increase with increasing breath-hold time and the slope of the deposition per unit time will be directly related to the mean airspace radius. The technique reveals differences in the deposition patterns between healthy volunteers and COPD-patients [44,45].

In **Paper 3**, this technique was compared to pulmonary proton density measurements in healthy volunteers. As expected, we observed a correlation between the distal airspace radius as assessed with AiDA and all measures of proton density with MRI.

3 Pulmonary Disease

3.1 COPD

The definition of COPD varies, but always include an *airflow limitation* associated with destruction of alveolar tissue (emphysema) [5,46]. The Global initiative for management of COPD (GOLD) include obstructive bronchiolitis [5] in the definition of COPD, whereas the "classic definition" include chronic bronchitis [46]. In short, COPD is a destruction of pulmonary tissue alongside a chronic inflammatory response.

Although some genetic factors predispose to COPD, such as the rare alpha-1 antitrypsin deficiency [47], the single most predictive factor is tobacco smoking. Although it is common knowledge that everyone who smokes does not develop COPD, there is likely a dose-response relationship where all smokers would develop COPD if they could smoke indefinitely [48].

The breakdown of tissue that is observed in COPD is likely mediated by inflammatory leukocytes, mainly macrophages and neutrophils [49], which perpetuate a vicious cycle of oxidative stress [50] and excessive protease activity [51] together with inhaled irritants.

The protease activity will eventually lead to tissue destruction and elimination of alveolar walls known as *emphysema,* which is histologically visible as an enlargement of airspaces distal to the terminal bronchiloes. The practical implication is that the tissue will lose elastic recoil and gas exchange surface – it is important to note that the pulmonary capillaries are part of the alveolar wall, thus emphysema is a destruction of the pulmonary capillaries as well.

The classic radiographic manifestation of COPD is low attenuation due to parenchymal destruction, low capillary blood volume and hyperinflation of the lungs. The reduction in $D_{L,CO}$ in COPD is primarily not an effect of increased membrane diffusion distance, but a loss of capillary blood volume.

3.2 Asthma

Asthma is another common disease that affects 10 % of the Swedish population [52]. It is characterized by airway hyperreactivity, hypertrophy of airway muscle and mucus glands, mucus plugging and the ensuing V/Q-inequality [46]. A very interesting feature of asthma is that it often presents with an elevated $D_{L,CO}$ [53,54]. This may be attributed to central bronchoconstriction, where the large negative transpulmonary pressure, needed to maximally inflate the lungs, result in an inflow of blood [55]. In contrast to COPD, asthma is commonly associated with symptom reversibility after bronchodilation (airway muscles relax), but it is a very heterogeneous disease [56].

From a MRI point of view, asthma may produce visible mucus plugs, bronchial hypertrophy and V/Q inequality.

3.3 Cystic fibrosis

Cystic fibrosis is one of the most common autosomal diseases in Sweden with an incidence of 1:5500 among new-born. Although the disease effects the whole body, the mortality due to airway dysfunction is over 90% [13]. The disease may be caused by a multitude of mutations on the cystic fibrosis transmembrane regulator (CFTR) protein, which is responsible for pumping chloride out of the cell. In the airways, this chloride transport is essential to make the mucus into a smoothly flowing liquid that can transport pathogens out of the lungs. In the CF patient, bacteria can easily colonize the thick, sticky mucus resulting in chronic infections. The constant bacterial presence attract neutrophils and macrophages into the distal airway, where inflammatory changes lead to collagen deposition and elastin degradation (fibrosis) [57].

Cystic fibrosis will result in mucus filled lungs, airway remodeling, fibrotic tissue, V/Q defects and increased membrane diffusion distance, which may be revealed in pulmonary imaging.

3.4 Pulmonary arterial hypertension

The pulmonary circulation is normally a low resistance system and in most healthy subjects the mean pulmonary arterial pressure (mPAP) is as low as 10-12 mmHg. Pulmonary arterial hypertension (PAH) is defined as having a mPAP of >20 or 25 mmHg (>25 mmHg in Sweden) which is near twice the normal pressure. The lung requires a very low pressure in order to maintain the very thin diffusion barriers of the

gas exchange capillaries and in many pulmonary diseases the capillary resistance is increased:

- Emphysema results in a smaller capillary bed and the resistance is inversely proportional to the number of capillaries that can be perfused.

- In the case of asthma, CF or other ventilation defects, the hypoxic vasoconstriction will increase resistance to direct blood flow away from un-ventilated areas.

- Chronic inflammation may induce neutrophil infiltration of vessel walls, which will be thickened.

All these changes and more will increase the resistance of the pulmonary circulation with a concomitant increase in mPAP. For example, in several studies of COPD the incidence of PAH was between 20 – 91 % [35,58]. The importance of the condition is easy to appreciate since a high mPAP will demand thicker vascular walls that successively increase the mPAP until right heart failure in inevitable. Indeed, in a cohort of COPD patients the mPAP increased by 0.4 mmHg annually [59].

Small vessel diameter is dependent of the perfusion pressure and a doubling of the capillary pressure will result in a 30% increase in capillary volume [13]. Moreover, an increase in the right descending pulmonary artery to >16mm and an increase in the diameter of the left descending pulmonary artery of >18mm has been shown a 98% sensitivity for detecting PAH [58]. If PAH leads to a distention of the entire pulmonary arterial vasculature, the precapillary blood volume will increase, and the non-oxygenated compartment will potentially dominate over the oxygenated lung blood compartment.

4   MRI of the Lung

Theoretically, the lung is arguably[1] the worst possible organ to analyze with MRI:

Per definition, a significant portion of the lung is air, which will not generate a MRI signal. In MRI, signal is already scarce, so a trade-off is made with imaging time, signal-to-noise ratio (SNR) and resolution. Accordingly, the same imaging protocol that successfully can be used in neuro-imaging will likely be useless in the lung.

The lung suffers not only from low proton density per se, but also susceptibility differences brought about by the airspaces. This reduces T2* which has been estimated to sub-milliseconds in mouse lungs [60] and 1.5 ms in the human lung [61].

Finally, although breath-holding can reduce motion artifacts it is not possible to arrest the heart for imaging purposes. Thus, images will contain a significant portion of cardiac motion artifacts, which, depending on the signal encoding scheme, may ruin parts or the entirety of the image.

4.1   The lung has low proton density

Low proton density invariably leads to a smaller and unfavorable signal to noise ratio (SNR) which consequently requires more imaging time or larger image voxels (low resolution). This thesis focuses on the Snapshot-FLASH which already operates at low resolution (128x64 pixels, interpolated) and thick slices (1.5 cm), to allow a very short echo time 0.7 ms. To further ameliorate the low proton density of the lung, this thesis work was preceded by some optimizations. In order to get the most signal out of a population of spins the echo time and flip angle must be optimized to the T_1. The optimal flip angle is known as the Ernst angle:

$$\alpha_E = cos^{-1}\left(e^{\frac{TR}{T1}}\right)$$

---

[1] Cortical bone may yield an even lower MRI signal due to the very rigid lattice, but is – in contrast to the lungs – very easy to keep still. Moreover, any damage to the bone will induce infiltration of blood and water, making bone injury ideal for MRI.

For TR=3.0 ms and T_1=1200 ms the Ernst angle is 4°. However, the FLASH sequence used a Gaussian excitation pulse which results in a Gaussian slice profile. This means that the nominal flip angle (4°) is only achieved in the very center of the slice. To counter this, a higher flip angle is used [62]. In-house optimization concluded that flip angles between 6-8° were optimal with respect to the coefficient of variation (CV) in repeated T1-measurements. Although a higher flip angle may lead to more SNR, the lower steady state magnetization causes severe inflow effects from the cardiac pumping [63], which was deemed to increase the CV.

Recent developments in MRI hardware and reconstruction algorithms have made ultra-short echo times (UTE) clinically available. This type of acquisition technique can potentially be implemented in any gradient echo sequence and is discussed further in chapter 11.

4.2   Susceptibility differences in the lung parenchyma

Magnetic susceptibility is an intrinsic property of all materials and indicate how it interacts with an applied magnetic field: a paramagnetic material will produce a stronger internal magnetization in response to an applied field, whereas a diamagnetic material will produce a weaker internal magnetization than the applied magnetic field. Generally, biological tissue is weakly diamagnetic and air (due to the paramagnetic oxygen) is weakly paramagnetic. Thus, in the lung there will be a field gradient between the airspaces (with a higher magnetic field) and blood vessels (with a lower field) where the magnetic flux density is not well defined. In these regions of *susceptibility differences,* there will be a fast dephasing of spins – the T_2^* is short. The mouse pulmonary T_2^* was 0.46 ms in wild type and 0.23 ms in an emphysema (tight-skin) model. The T_2^* of healthy human lungs have been estimated to 1.47 ms at expiration and 1.45 ms at inspiration [61,64].

Conventional MRI sequences in the lung should be optimized for minimal echo time, which often requires thick slice profiles or volumetric imaging. Indeed, the use of slab selective pulses plays a double purpose since the total SNR is vastly increased and very short TE becomes possible. Fast spin-echo imaging is another way around the short T_2^*, however, due to the simultaneous flow/diffusion of blood, the signal becomes dependent on the inter echo spacing [65].

4.3   Lung MRI suffers from respiratory and cardiac motion

Respiratory motion is somewhat trivial in imaging since even basic chest x-ray requires the subject to hold their breath. On the other hand, an MRI examination may take in excess of 40 minutes to complete and intermittent breath holding will be strenuous and tedious. The protocol used in this dissertation contained automatic breath hold instructions (a recorded voice that is played by the scanner software before each scan) because this minimized motion noise altogether.

Gating is another option that can be employed in several clinical protocols, and allows the subject to breathe freely. Prospective gating refers to using some kind of navigator – a waistband that records the breathing motion of the patient, or a navigator echo that records the position of the diaphragm. By using the available information, the scanner software determines when the imaging sequence should commence.

Retrospective gating can be performed by continuously collecting MRI data and retrospectively sorting the signal into different respiratory phases. Although this sounds like a good idea, it comes at the cost of additional image noise, which can be devastating in the low-SNR lung parenchyma (Figure 5).
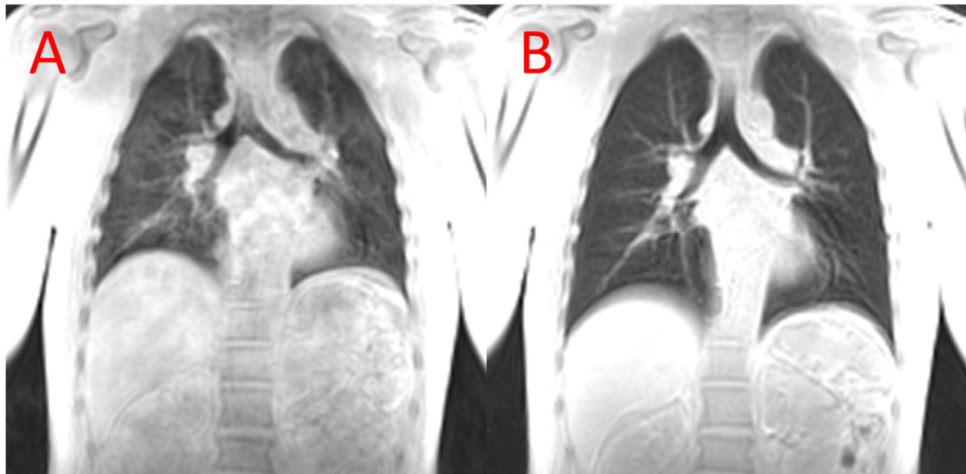
Figure 5 Comparison between prospective gating (A) and breath hold (B) in a UTE scan with spiral read-out. The motion generated noise is spread over the whole image, ruining the low signal lung parenchyma in (A). In (B) only cardiac motion and a minor diaphragm shift is visible.

Cardiac motion is the final hurdle and has been controlled by the use of very fast gradient echo sequences in this thesis. A single FLASH-image takes 200 ms to acquire and 16 images are used to reconstruct a T_1-map (see section 8.2), consequently, cardiac motion artifacts are inherently filtered by the reconstruction – as discussed in section 4.1. An interesting alternative is to use a modified Look-Locker inversion recovery (MOLLI) which is in fact developed for T_1-quantification in the heart, by triggering at specific time points in the cardiac cycle [66]. This sequence is based on a balanced steady-state free-precession acquisition and did not generate enough signal to be useful in the lung parenchyma in our in house tests, but may be modified to fit lung imaging in the future.

5 Magnetic relaxation in blood

Whole blood consist of 33-49% (volume) red blood cells and contain 7-10 mmol/liter hemoglobin (or 20-22 mmol/l inside the RBC) [67]. Water diffuses relatively freely across the RBC membrane to interact with the intercellular hemoglobin. Thus, T_1- and T_2-relaxation in blood is dominated by the hemoglobin concentration which varies with age, sex and smoking status [68,69]. In the deoxygenated state, as in systemic venous blood, hemoglobin iron is paramagnetic and very effective at inducing relaxation. In the oxygenated state, the Hb-iron is diamagnetic and relaxation is less effective. However, during pure oxygen breathing free molecular oxygen acts to enhance relaxation as outlined in chapter 7. Blood T_1-relaxation can be understood by the processes outlined in this chapter:

- Blood relaxation can be described as water exchange between erythrocytes and plasma [70]

- Blood relaxation depends on both diamagnetic and paramagnetic effects of hemoglobin [70]

- Susceptibility effects should be considered when interpreting blood/pulmonary T_1-quantification [20,71]

- The T1 of blood is longest at physiological arterial oxygenation levels (100 mmHg) [19]

5.1 Blood relaxation rates is a weighted average of relaxation in the RBC and plasma

Water exchange is integral to the understanding of MRI relaxation and is the principal mechanism different spin populations are interacting. For example, water exchange between the hydration sphere of a contrast agent and the bulk water result in a large bulk relaxation effect, even though a very small number of water molecules are affected by the relaxation agent. Although cell membranes are generally impermeable to water, RBC contain sufficient aquaporins (AQP1) to facilitate almost free diffusion [72].

Li et al. 2015 presents an exchange model to describe relaxation in blood as a function of plasma protein, Hb, oxygenation and field strength [70]. The major spin populations in whole blood are erythrocyte versus plasma water, where water molecules will spend an average of 10 ms in the erythrocyte (although this values very recently was re-estimated to 19 ms [73]). This means that the exchange rate k_{ex} = 50-100 s-1 between the RBC and plasma pools is faster than the difference in relaxation rate between the pools:

$$k_{ex} \gg |R_{1,RBC} - R_{1,plasma}|$$

Under the above assumption of fast exchange, the effective relaxation rate will be the weighted average relaxation rate of the two water populations: plasma-water and RBC-water. If the fraction of water inside the RBC is called f_{RBC}, it is possible to calculate the following effective relaxation rate, R_1:

$$R_1 = f_{RBC}R_{1,RBC} + (1 - f_{ery})R_{1,plasma}$$

Thus, we can generally treat blood as having a single relaxation rate, linear in the concentration of hemoglobin. A typical example of this, is that females generally have lower hemoglobin and thus longer T_1 values, a finding confirmed in left ventricle blood in vivo [74]. This difference between men and women diminish with age, since women gain more hemoglobin after menopause and men loose hemoglobin due to decreasing testosterone levels with age [67], as can be seen in Figure 6.

5.2 Hemoglobin relaxation contain three paramagnetic and diamagnetic contributions

At 3 Tesla the diamagnetic relaxivity of hemoglobin $r_{1,dia,Hb}$ is $62.9\ (mol/kg\ s)^{-1}$ and the paramagnetic relaxivity of deoxyhemoglobin $65.6\ (mol/kg\ s)^{-1}$ [70]. This means that deoxy-Hb will be twice as effective at inducing T_1 relaxation compared with fully oxygenated hemoglobin.

Although a substantial part of the blood paramagnetic relaxivity comes from deoxy-Hb, there is also a paramagnetic contribution from methemoglobin. While the molar relaxivity of methemoglobin is 20 times that of hemoglobin $r_{1,para,metHb} = 1260\ (mol/kg\ s)^{-1}$ [70], the concentration is in the 0.5% range in healthy individuals [75], resulting in a 10% increase in relaxation rate compared to the diamagnetic hemoglobin contribution alone. Methemoglobinemia (elevated levels of met-Hb in the blood) will potentially have a substantial effect on blood-T_1 (and thereby pulmonary-T_1); and

although this is a rare condition, methemoglobinemia may be induced by some medications [76].

In conclusion, the diamagnetic and paramagnetic contribution of Hb and deoxy-Hb are equal in magnitude and the paramagnetic met-Hb contribution is smaller but significant. The magnitudes of each contribution varies with field strength, but the proportions remain roughly the same at clinical field strengths [70].
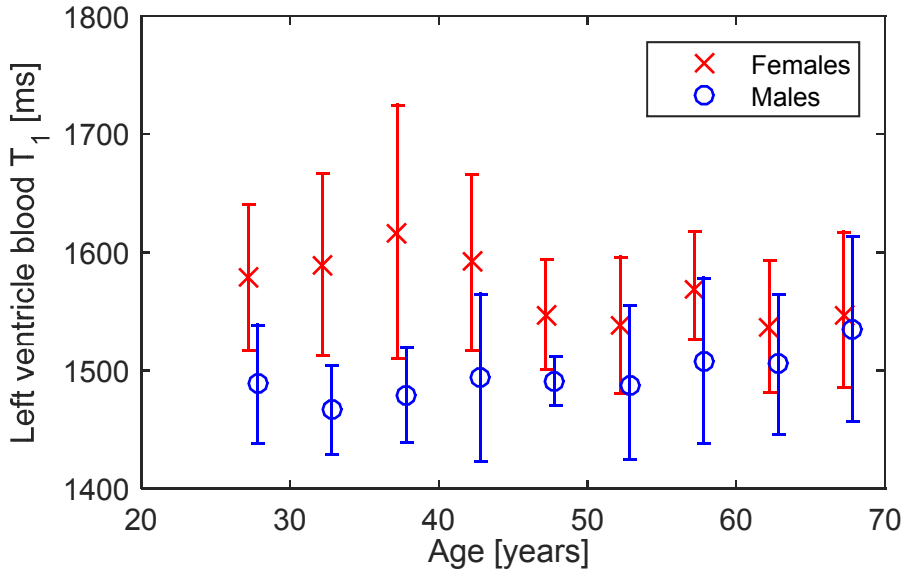
Figure 6 Left heart blood T_1 as a function of age and sex, adopted from Piechnik 2013 [74] . In the fertile age, men and women will have significantly longer blood T_1 due to differences in hemoglobin. With age, these differences disappear.

5.3 Deoxyhemoglobin modulate blood susceptibility and T_2^*

Blockley and Spees et al. both consider relaxation in blood as a function of paramagnetic deoxyhemoglobin which effects both relaxation times and the susceptibility of blood [20,71]. This means that as the oxygen content varies within physiological range, the susceptibility difference between RBC and plasma will vary and at 95% oxygen saturation the plasma and erythrocyte susceptibility will be matched; T_2^* will be the longest; and the signal increase [20]. Theoretically, the addition of a paramagnetic contrast agent to blood can induce a susceptibility matching

between deoxy-erythrocytes and plasma, which would yield a counter intuitive T_2^* dependent signal increase [71].

This does not happen during OE-MRI where susceptibility effects from oxygen have been shown to be $\Delta\chi = -0.02\ ppm$ in fully oxygenated plasma, such that any important susceptibility effects will be mediated by deoxyhemoglobin. However, we know that the inhalation of 100% oxygen does decrease T_2^* in the lung [61], probably due to induced susceptibility differences between oxygen filled airspace and diamagnetic blood.

5.4 Blood T_1 relaxation is fastest at very low or very high oxygen concentration

Silvennoinen et al. is the only record, to the knowledge of the author, of blood relaxation rates in both hypoxic and hyperoxic conditions, which makes it very relevant for this discussion Figure 7 [19]. Healthy venous blood has a pO2 of 40 mmHg and can go up to 60 mmHg during 100% oxygen breathing, this corresponds in a difference in oxygen saturation from 75% to 90% which means that we will have a *lower* relaxation rate in venous blood during an OE-experiment, contributing to a *negative* OE-effect measured with T_1 end-points. This can be seen in the inferior vena cava of healthy individuals [77], or in the zero enhancement regions of PAH-patients [78].

However, according to the previous paragraphs, venous blood may exhibit some signal increase due to longer T_2^* if we use a signal enhancement end-point. This is one of the reasons that T_1-quantification was chosen as the primary OE-endpoint in this thesis.
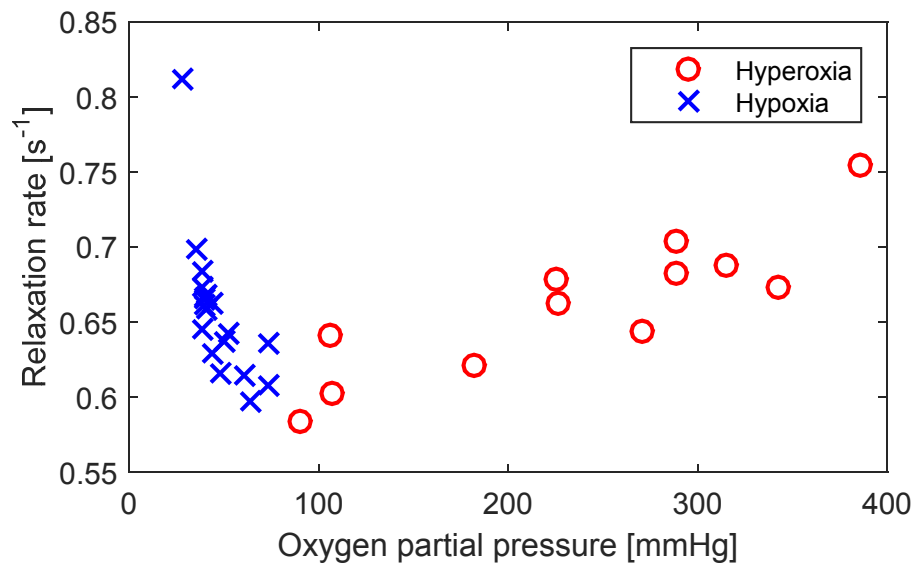
Figure 7 Plot of the relaxation rate of blood as a function of oxygen saturation, with data from Silvennoinen 2003 [19]. T_1 is longest at physiological oxygenation (100 mmHg oxygen) and relaxation will be more effective at both high and low oxygen concentration: in hyperoxia due to paramagnetic oxygen – in hypoxia due to paramagnetic deoxy-Hb.

6 Plasma proteins

Blood-T_1 has been shown to vary with age and sex, in a manner that cannot be explained by EVF alone [67,74]. Plasma proteins of special interest from a MRI perspective are diamagnetic albumin, Immunoglobulin G (IgG) and fibrinogen, as well as paramagnetic transferrin and ceruloplasmin which are presented with typical concentrations in table 1.

Table 1 The 13 most prominent plasma proteins according to concentration and references.

Protein	Conc. [g/dl]	Reference
Albumin	4.5	Weaving [79]
Immunoglobulin G	1.1	Gonzales-Quintela [80]
Fibrinogen	0.3	Tarallo [81]
Transferrin	0.25	Denko [82]
Alpha1-antitrypsin	0.25	Denko [82]
IgA	0.25	Gonzales-Quintela [80]
C3+C4	0.15	Ritchie [83]
IgM	0.15	Gonzales-Quintela [80]
LDL Cholesterol	0.15	Wahl [84]
Haptoglobin	0.1	Shahabi [85]
α1-acid glycoprotein	0.1	Denko [82]
HDL Cholesterol	0.05	Wahl 1981
Ceruloplasmin	0.04	Denko [82]

Albumin is the major diamagnetic protein in plasma (approx. 4.5 g/dl), varies considerably with age and sex, with the difference in sexes being largest between 20-40 years of age [79,82]. Concentrations of IgG (1.1 g/dl) and fibrinogen (0.3 g/dl) are both increasing from 20 to 60 years of age and are marginally higher in females [80,81]. The relaxivities of these proteins are similar and approximately 0.035 (g/dl)$^{-1}$ s^{-1} [86] and their total contribution to plasma relaxation is approx. $R_{1,proteins} = 0.2\ s^{-1}$.

Transferrin (analogous to total iron binding capacity, TIBC) is the major paramagnetic plasma protein (approx. 0.25 g/dl) and can bind up to two Fe(III) ions per molecule. Concentration is age and sex dependent [82]; and iron saturation is sex dependent [87]. Yilmaz et al. 2004 determined the relaxivity of transferrin iron (TIBC x saturation) to 2.4 s^{-1}mM^{-1} [86] and the contribution of transferrin to plasma relaxation rate is approx. $R_{1,trf} = 0.05\ s^{-1}$.

Ceruloplasmin (approx. 0.04 g/dl) contains 6 copper atoms per molecule, of which 40 % are in the paramagnetic Cu(II)-state [88]. Due to its role in the iron metabolism, ceruloplasmin concentration is both age and sex dependent [82]. There is no work presented on the relaxivity of ceruloplasmin at modern MRI field strength, but the relaxivity of Cu(II) in protein solutions is 1.68-2.18 s^{-1}mM^{-1} [18]: The theoretical contribution of ceruloplasmin to plasma relaxation would be in the order of $R_{1,crl} = 0.01\ s^{-1}$.

With these five proteins most of the variation in plasma T$_1$ with age and sex can be accounted for. Contribution from the rest of the plasma proteins, including ferritin (approx. 10 μg/dl), are regarded as physiological noise. Among the inorganic plasma constituents, none can compete with iron regarding paramagnetic contribution. However, potassium, phosphorous and protein bound calcium exhibit substantial variation with age and sex [89–91], and may contribute with relaxation pathways which remains to be investigated.

7 Paramagnetic relaxation of molecular oxygen

The MR relaxation rate in biological fluids has been claimed to be a linear function of oxygen tension [11,92–94]. This assumption is based on Henry's law, which states that the molar amount of gas in a solution is linear in the gas partial pressure at the water-gas interface, and a single measurement of oxygen relaxivity in distilled water [12]. This simplified model of oxygen T_1-relaxation has three major faults:

- All paramagnetic contrast agents undergo field dispersion, meaning that the relaxivity must decrease with increasing field strength. The field dispersion of oxygen occurs between 0.5-7 T and has a maximum negative slope around 1 T.

- Oxygen solubility is a function of electrolyte, protein and cell content – the amount of dissolved gas at a given oxygen pressure will thus vary with the composition of the fluid.

- Paramagnetic relaxivity depends on other solutes, so the same amount of dissolved gas will produce different relaxation enhancements depending on the composition of the fluid.

7.1 Oxygen electrons have a short correlation time dominated by electron T_1-relaxation

The molecular form of oxygen that we breathe, O_2, or dioxygen, has two unpaired electrons in the p orbital. In the general case two spins would pair up and cancel, but in the oxygen molecule it is energetically favorable to fill the shell with single spins, yielding a net magnetic moment corresponding to the electron spin. The electron has a large gyromagnetic ratio and can interact with proton spins through dipole-dipole interaction [95,96]. The relaxation effectiveness in turn depend on the electron spin correlation time, which tells us how long, on average, an electron keeps the same polarization from the viewpoint of the proton. The electron correlation time τ_C is a combination of three terms: the electron's own longitudinal relaxation time ($T_{1,e}$); the

rotational correlation time of the electron-proton spin interaction τ_R (is the electron or proton part of a fast or slow tumbling macromolecule?); and the chemical exchange rate τ_{CE} (is the proton competing with other protons for the paramagnetic center?):

$$\tau_C{}^{-1} = T_{1,e}{}^{-1} + \tau_R{}^{-1} + \tau_{CE}{}^{-1}$$

To determine the main contribution to the electron correlation time, the dispersion profile was recorded in several solvents of different viscosity [97]. The correlation time was calculated by fitting the Solomon equation for a two-spin system to the dispersion data of the oxygen solutions [98]:

$$R_1 \propto \frac{\gamma_e^2 \gamma_p^2}{r^{-6}} \tau_c \left[\frac{1}{1 + (\omega_p - \omega_e)^2 \tau_c^2} + \frac{3}{1 + (\omega_p)^2 \tau_c^2} + \frac{6}{1 + (\omega_p + \omega_e)^2 \tau_c^2} \right]$$

Interestingly, the viscosity of the solvent had minor effect on the dispersion indicating that the correlation time is governed by intramolecular T_1-relaxation in the oxygen molecule. Moreover, the electron T_1 was estimated to 5-10 picoseconds according to the most recent data [97].
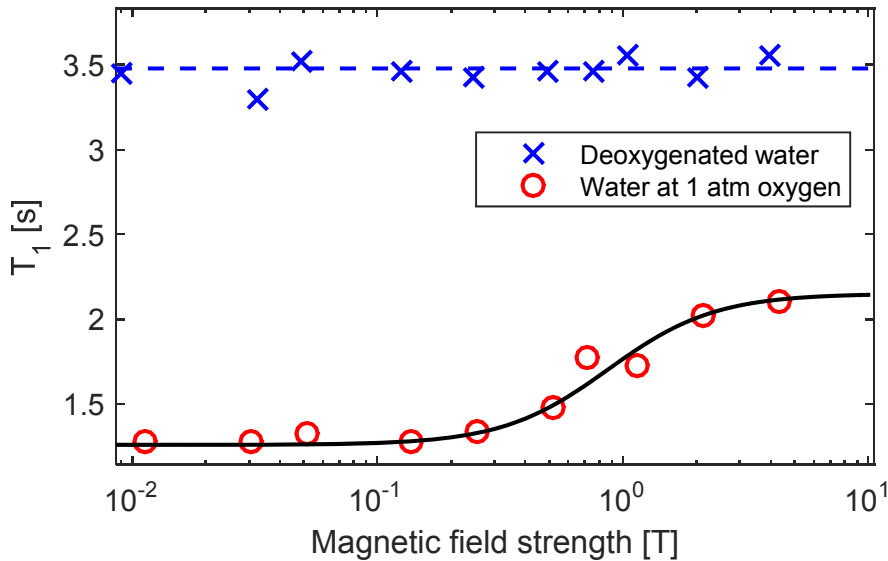
Figure 8 Data from Graf et al. 1980 [99] is fitted with a dispersion curve assuming an electron correlation time of 60 ps. Experiments conducted 20 years later indicate that the correlation time is 5-10 ps (Teng et al. 2001 [97]). Nevertheless, the relaxivity of oxygen does decrease by a substantial amount between 0.2 and 5 Tesla.

The traditional MRI contrast agent Gd^{3+} has an electron T_1 of 1-10 ns, which is 1000 times longer than the oxygen molecule $T_{1,e}$, and makes Gd^{3+} a very efficient relaxation agent. The electron T_1 is dependent on intramolecular spin-orbit couplings, vibrational phonons (Raman and Orbach processes), and distortions from intermolecular collisions [100].

In conclusion, the field dispersion of paramagnetic oxygen dictates that the relaxivity is field strength dependent, as per Figure 8, and the relaxivity seems to be insensitive to the solute viscosity.

7.2 Oxygen is poorly soluble in water but non-polar proteins and cell walls increase solubility

From the previous discussion it would seem that oxygen is a powerful relaxation agent in water – if the effective relaxation time becomes T_{1e} = 5 ps instead of the water proton relaxation time T_1 = 5 s^{-1} this is a factor of 10^{12}! However, oxygen is a non-polar molecule making it poorly soluble in water and the hydrogen bond disruption between water molecules makes it even less soluble at physiological temperatures. Although most salts will further decrease the solubility of oxygen in water, the addition of non-polar protein residues and domains, as well as the hydrophobic parts of membranes, increase the solubility [101].

This is the exact opposite of Henry's law – the same partial pressure of oxygen will lead to more oxygen being dissolved in a cell suspension, than in distilled water.

7.3 Paramagnetic relaxation effects are mediated and enhanced by protein

Most paramagnetic contrast agents interact favorably with macromolecules and exhibit a higher relaxivity in higher macromolecule concentrations [16,17,102,103]. Moreover, the magnitude of this effect varies between different plasma proteins [18]. The same is true for molecular oxygen, which will associate with low affinity to protein residues and produce relaxation enhancements between 0.1 to 60 s^{-1} at these sites [104]. The water proton relaxation enhancement at the residue is transferred to the bulk water by chemical exchange or by water exchange as usual.

Blood plasma contain salts and proteins but no cells (per definition), making oxygen less soluble in plasma than in water [101], however, the protein content still make the oxygen relaxivity higher in plasma ($3.38 \cdot 10^{-4} s^{-1}$ $mmHg^{-1}$ [105]) than in distilled water

(2.49·10^{-4} s^{-1} mmHg^{-1} [12]). Erythrocyte enriched blood (hct=0.6) have also been shown to have a higher relaxivity for oxygen (4.38·10^{-4} s^{-1} mmHg^{-1} [105]) than regular whole blood (4.1 s-1 mmHg^{-1} [19]). This can be generalized by considering the erythrocyte water and plasma water as proton pools in fast exchange [70] and using a higher value for the oxygen relaxivity in the erythrocyte interior. This model, which was developed but never presented as part of this thesis, is depicted in Figure 9 and estimates the intra-erythrocyte relaxivity to 5.99·10^{-4} mmHg^{-1} s^{-1} using data from two sources [19,105].
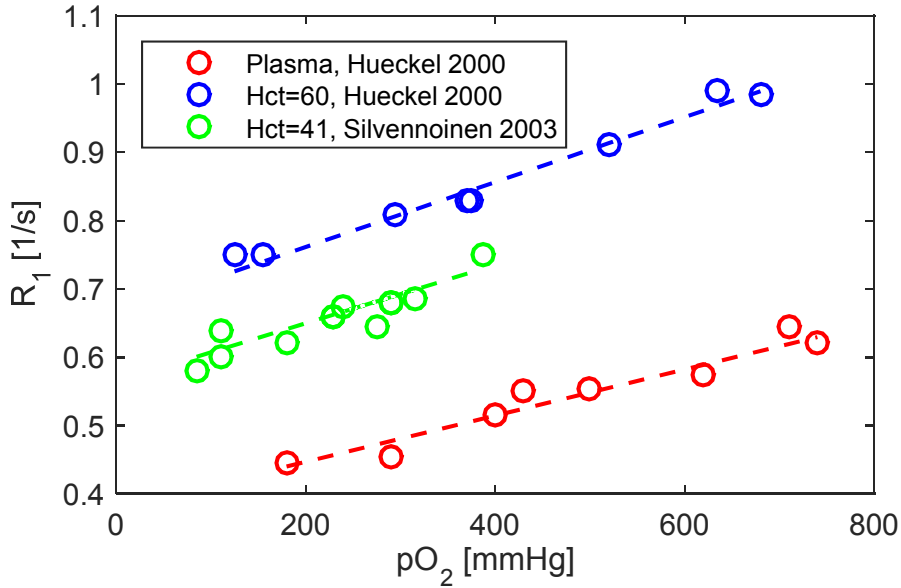
Figure 9 Using different values for the oxygen relaxivity in blood and erythrocytes, we can combine the hyperoxia-measurements of Hueckel [105] and Silvennoinen [19]. A single fast exchange blood model [70] is used to fit all data points using one oxygen relaxivity value for blood plasma: 3.38·10^{-4} mmHg^{-1} s^{-1} and a high value for the erythrocyte interior 5.99·10^{-4} mmHg^{-1} s^{-1}

8   T$_1$-Quantification

From the previous discussion we know that dissolved oxygen in blood will effect both T$_1$ and T$_2$* making changes in signal intensity difficult to predict. Although we know now that oxygen relaxivity is a function of field strength, solubility, protein content and cell content, the vastly simplified equation for the OE-effect is nonetheless true:

$$R_{1,blood} = R_{1,0} + r_{1,oxygen}P_{O2}.$$

This means that any attempt to quantify the OE-effect must start with a quantification of individual relaxation rates.

8.1   Inversion recovery

The most straightforward way to measure T$_1$, and what can be considered as the gold standard in imaging, is the 2D spin echo inversion recovery experiment. After an initial 180 degree RF pulse, to invert the z-magnetization, free T$_1$-recovery is allowed during the inversion time (TI). At the inversion time, a regular spin echo or turbo spin echo sequence is used to sample the magnitude of the resultant z-magnetization (Figure 10 A). Repeated measurements with different TI result in a magnetization recovery curve as indicated in Figure 10 B. If the repetition time (TR) is kept constant, T$_1$ can be calculated from a simple 3 parameter fit on the following form [106]:

$$S(TI) = a - b \cdot \exp\left(\frac{-TI}{T1}\right)$$

For a perfect inversion pulse the parameter *b* should equal to 2*a*, since the magnetization is inverted at time zero. Making this assumption may make the fitting algorithm faster, but less precise.
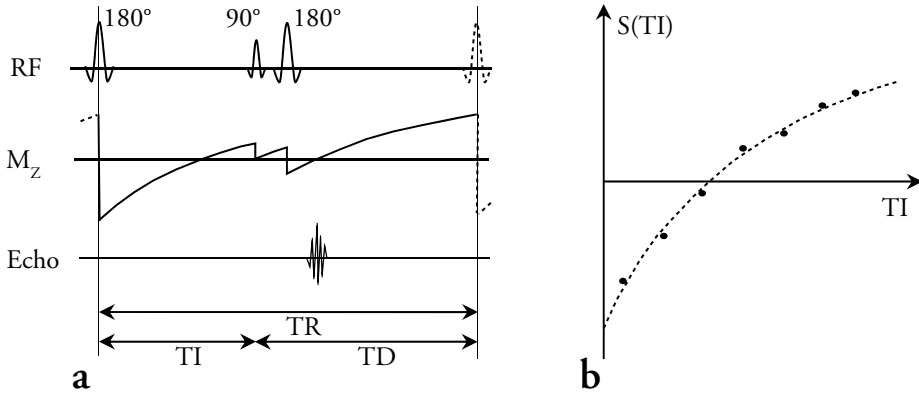
Figure 10 A.Schematic drawing of the IR-SE sequence, with 180 and 90 degree pulses. **B:** The signal intensity (S) as a function of inversion time (TI) in the inversion recovery experiment, fitted with a curve on the form $S(TI) = a - b \cdot \exp(-TI/T1)$. Figure © Siversson [107] with permission.

A special case of the IR-SE is the IR-HASTE, (IR- Half-Fourier Acquisition Single-shot Turbo spin-Echo) in which a spin-echo train is used to sample half the Fourier space in one shot (generating a full image due to the redundancy of Fourier space). The sequence can be used slice selectively and interleaved for very fast imaging and is standard software on all clinical scanners, making it attractive for T_1-measurements. However, it is known that slice selectivity of the inversion pulse will make the sequence more sensitive to blood flow in the lung, since inflowing blood will give rise to a more positive signal than free T_1-recovery [108].

8.2   Look-Locker T_1-quantification

One of the most widely used methods for T_1-quantification, and the method employed in this thesis, is the Look-Locker method [109], based on fast gradient echoes and adopted for imaging purposes by Brix et al [110]. Compared to the IR-SE variations that need several inversion times for a single T_1 calculation, the Look-Locker sequence samples all images during one inversion and can thus create a single-slice T_1-map in 3-5 seconds [111].
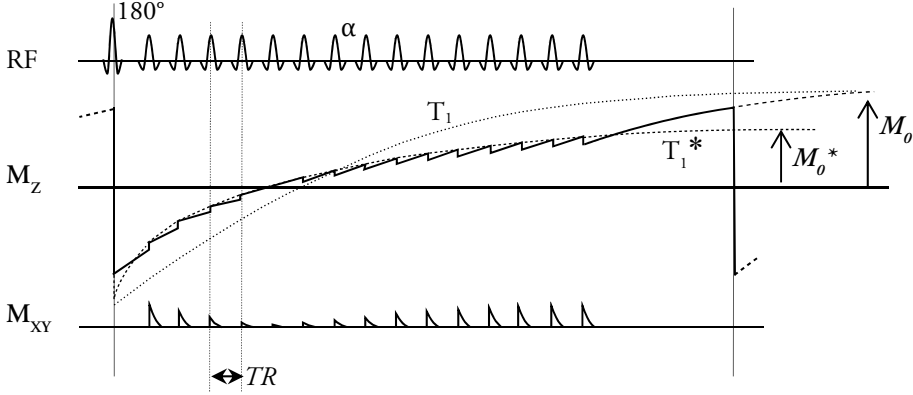
Figure 11 Schematic drawing of the Look-Locker sequence. A series of low flip angle gradient echoes are used to continuously sample the magnetization recovery. RF is the radio frequency 180 degree or low angle shots; Mz is the recovering Z-magnetization, and Mxy is the transverse magnetization which is the recordable signal. In reality more than 1000 low angle RF pulses are applied to acquire a single T1-map during 3 seconds, but in the figure there are only 15. Figure © Siversson [107] with permission.

After the initial global inversion pulse, a series of gradient echoes are continuously collected during the z-magnetization recovery, with such low flip angle α that the recovery is only slightly disturbed, until a gradient echo steady state is reached. The low angle flip pulses will make the recovery apparently faster, which is denoted by the apparent T_1, or T_1^*. Likewise, the final magnetization will be the steady state magnetization M_0^* instead of the fully recovered equilibrium magnetization M_0. The value of T_1 can be calculated analytically as follows [112]:

$$\frac{1}{T_1} = \frac{1}{T_1^*} + \frac{\ln(\cos(\alpha))}{TR}$$

However, unless specifically measured, the effective flip angle in the tissue is unknown. This was the focus of the dissertation of Siversson 2011 [107] and the practical consequence is that T_1 is best calculated from a three parameter fit to the Look-Locker signal.

$$S(t) = a - b \cdot \exp(-t/T_1^*)$$

Under the assumptions that TR<<T_1; that full magnetization recovery is allowed between inversions; and that the inversion pulse is perfect, the above parameters is used to calculate T_1 as [112]:

$$T_1 = T_1^* \left(\frac{b}{a} - 1\right) = T_1^* \frac{M_0}{M_0^*}$$

Fortunately, the two first assumptions are easily satisfied in clinical lung imaging, but a few percent lower T_1 can be expected due to inversion pulse imperfections. Moreover, if a time efficient protocol is preferred as in **Paper 1 and 2**, a steady delay time can be used between inversions and the T_1 can be easily and accurately calculated using an iterative algorithm [62].

8.3   The use of selective or global inversion pulses

An important consideration is the choice of global or slice selective inversion pulses in pulmonary T_1-quantification. The quantification procedure is based on an inversion, a waiting time and a recording of the signal, as outlined in the previous section. If there is extensive blood flow into the imaging slice, the originally inverted spins will leave the slice and be replaced by fully recovered spins. This will lead to an artificially fast T_1-relaxation. In the case of pulmonary MRI, the estimated T_1 will be approximately 200-300 ms lower [113,114].

The implementation of the Look Locker quantification used in this thesis routinely offers both slice selective and global inversion pulses. However, since spin-echo techniques are often used in an interleaved manner (multi slice), global inversion pulses may be disabled on the scanner and some modification of the protocol is required. Early T_1-measurements in the lung reveal surprisingly low T_1, which may be attributable to the use of selective inversion pulses [8,115].

Even after using a global inversion pulse it is important to note that the pulmonary transit time – the time it takes blood to pass from the right to left ventricle – occurs on the same time scale as the longest inversion times used in T_1-quantification. If the study subject is fully at rest, with a cardiac index of <5 l m^2 min^{-1}, the transit time is around 6 seconds and non-inverted blood is not expected to reach the lung parenchyma within the inversion experiment. However, if the cardiac output is only slightly elevated due to stress, the pulmonary transit time will decrease to 2-3 seconds very quickly [116] and all T_1-measurements must be considered to be influenced by flow at long inversion times.

Some attempts have been made to quantify flow with the T_1-shortening associated with slice selective inversion pulses. This is a form of arterial spin labeling (ASL) and is sometimes referred to as FAIR (flow sensitive alternating inversion recovery) [114]. The most recent report established a 7-11 % decrease in pulmonary perfusion during hyperoxia in mice [117].

9 Pulmonary T_1 as an imaging biomarker

In the search of small but clinically relevant changes (such as response to a new drug) parametric MRI is preferred over classic T_1- or T_2-weighted MRI. This is because MR images will always inherent properties of all relaxation times, proton density, flow effects, scanner parameters and minuscule day-to-day variations in magnetic field homogeneity. Parametric imaging tries to isolate at least the most obvious parameters which we know have clinical relevance – e.g. a "signal enhancement" in a T_1-weighted image does not tell if the signal increase is due to a higher flow, more blood or lower T_1.

9.1 Pulmonary T_1-depends on the echo time

Triphan et al. 2014 quantified T_1 relaxation in excised, bloodless porcine lung and found it to be 661 and 616 ms in two samples [118]; we also know that the T_1 of human blood is typically 1500-1600 ms [74]. Triphan et al. 2015 later established that T_1 of healthy human lung is an echo time dependent weighted average of the parenchymal T_1 and the T_1 of blood [119]. For T_1-experiments with conventional echo times (>1 ms) the measured T_1 is 1200-1400 ms, and for read-outs with UTE (TE=70 μs) the T_1 is between 950-1150 ms (Figure 12). In **Paper 1**, measurements were performed at tidal inspiration, yielding a slightly lower T_1 than predicted by Triphan [119]– the mean T_1 for males was 1150 ms at an echo time of 0.7 ms.
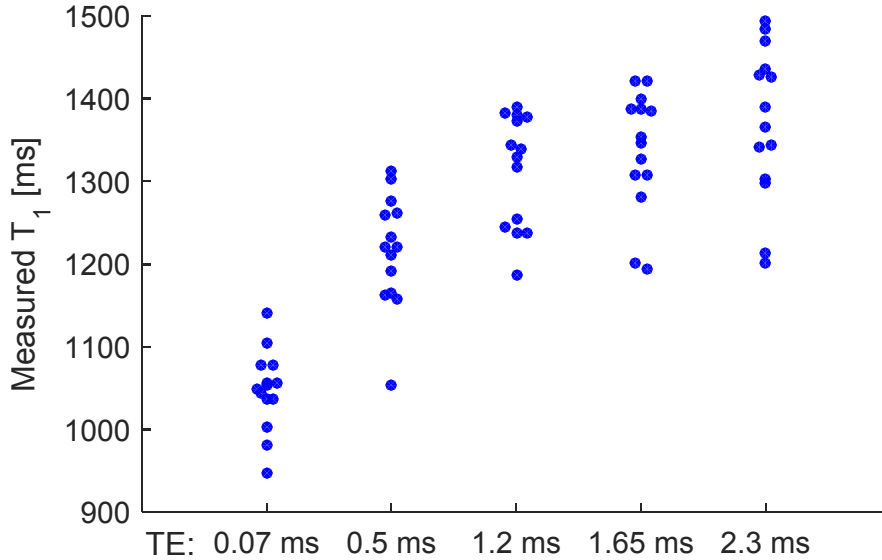
Figure 12 Pulmonary T_1 in 12 subjects measured with a segmented Look-Locker sequencewith different echo times. Data from Triphan et al. 2015 [119]. The echo time used in **Paper 1-4** was 0.7 ms.

9.2 Pulmonary T_1 is different when measured with spin- or gradient-echo

Although a recent meta-analysis concluded that there is no systematic difference in T_1 estimated with a spin echo or gradient echo [93], this question is raised in **paper 4** of this thesis. Indeed, in the meta-analysis there is no difference in means between spin-echo and GRE type sequences at p=0.95. However, two early FSE measurements report T_1 values of 900 ms in healthy volunteers, which is typical of slice-selective measurements known to result in very low T_1. By discarding those and adding the measurements presented in **Paper 4**, there is definitely reason to consider a systematic difference between FSE and Look-Locker based T_1-quantifications in the lung. In fact, a bootstrap power calculation give this data set a 50% chance to detect a significant difference. The meta-analysis data is presented in Figure 13, with a 95% confidence interval for difference in mean T_1 between the methods of [-2.9, 170] ms, and implies a higher T_1-value in FSE measurements. The direct comparison in paper 4 reveal a significant difference in mean T_1 between FSE and LL measurement with a 95% CI of [29, 161] ms at p=0.0075.
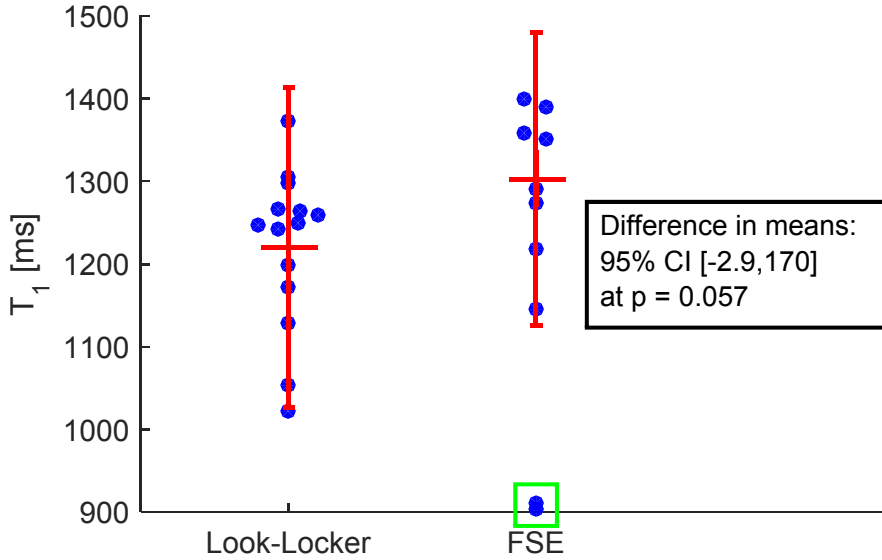
Figure 13 Meta-analysis of pulmonary T_1 values from Dietrich et al. 2017 [93], with two additional group means from Paper 4 and two FSE data points excluded as outliers (green square), give us reason to believe that there may be a systematic difference between Look-Locker and FSE quantification of T_1.

A potential explanation for the higher T_1 in FSE-based imaging (and the higher ΔR_1 as will be seen in the next chapter) is the capillary blood volume, which will experience the greatest susceptibility gradient in the lung. If the capillary blood does not contribute to the GRE signal due to the very steep susceptibility gradient, but contributes to the FSE signal, the FSE will measure a higher T_1. Moreover, there is reason to believe that capillary blood has a higher T- than other blood pools, because of the Fahreus effect, which predicts that capillary blood will contain a smaller fraction of RBC [120].

9.3 Pulmonary T_1-depends on lung inflation and the age and sex of the studied subject

It was previously established that the T_1 of a blood-less porcine lung is approximately 650 ms [118], it is thus reasonable that any decrease in pulmonary blood volume in a normal lung will lead to a lower T_1. During inspiration, the pulmonary blood volume is reduced and T_1 is consequently lower at inspiration than expiration [121]. In fact, vascular resistance is at a minimum at tidal breathing and highest at TLC [4] and capillary width decrease with transpulmonary pressure (inflation pressure) [13]; thus lung blood volume is lower during hyperinflation (inflation beyond tidal breathing)

[122]. The difference between full inspiration and expiration is 134 ± 113 ms, where the inspired state has a lower T_1 [121].

In **Paper 1,** the dynamics of pulmonary blood, lung volumes and the age-dependent shifts in blood EVF was used to explain changes in lung T_1 with age and sex in a 1.5 T clinical scanner [123]. The take home message is that healthy lung T_1 is approx. 1250 ms in young females and 1150 in males and females over 50 years of age. This paper is still the largest published record of T_1 measurements in healthy human lung; in a meta-analysis on pulmonary T_1-measurement from 2017, the material from **Paper 1** constitute 16 % of the total number of measurements [93].

Figure 14 Pulmonary T_1 as a function of age for males and females from **Paper 1**. Young females have a significantly longer T_1 than all other subjects. Compare this graph to Figure 6: left heart blood as a function of age and sex.

In the material, consisting of 30 subjects evenly distributed between age and sex, there was a striking difference in pulmonary T_1 between young females and all other subjects (p<0.001). This is attributed to differences in blood EVF and blood T_1 [67,74]. Moreover, both men and women will increase their RV and subsequently breathe at a higher volume with increasing age [27]; leading to a displacement of lung blood [124]; which creates two concurrent effects (lower lung blood, higher inflation [121]) to lower T_1 at a high age.

9.4 Pulmonary T_1 is lower in COPD

In the excellent thesis by Dr Daniel Alamidi it was shown that T_1 is shortened in COPD patients compared to healthy controls; that T_1 was shorter in severe compared to moderate COPD; and that T_1 was significantly correlated with both FEV/VC and k_{CO} (r>0.7, p<0.0001, n=36) [125]. The reduction of T_1 in COPD can be interpreted in terms of tissue destruction; distention and compression of the capillary sheet; and subsequent decline in blood volume. In particular, $D_{L,CO}$ is a function of capillary blood volume [40], which we know decrease in COPD and will directly affect T_1 according to the previous discussion about blood volume. The correlation between FEV/VC and T_1 can also be explained in terms of tissue destruction; where emphysema will induce premature compression of airways and thus respiration at a higher lung volume, which is associated with lower T_1. A later study confirmed the findings that COPD patients have lower T_1 than healthy controls and that asthmatics have T_1 between that of COPD and healthy lungs [126].

9.5 Pulmonary T_1 may reveal perfusion deficits and fibrosis

In an interesting study T_1-quantification, OE-MRI and contrast enhanced perfusion (Gd-DTPA) were all performed in 20 COPD patients, with regional abnormalities used as an end-point. Across all regions, T_1-abnormality correlated with perfusion defects (r=0.8), as well as GOLD stage (r=0.45) [127], supporting that notion that T_1 measurements can reveal lung perfusion deficits.

Similar results were found in a 2004 study of cystic fibrosis patients – pulmonary T_1 shortening correlated to low perfusion areas, although the study was qualitative and limited to five CF patients [128].

A pilot study conducted early in this thesis work analyzed T_1 maps from 5 women who received radiation treatment for breast cancer 10 years earlier (presented as a poster at IWPFI, Edinburgh 2015 [129]). The dependent lung regions received >30 Gy radiation dose and had visible fibrosis on CT images, which is known to be associated with reduced T_1 [130]. Compared to the controls, the group who received radiation treatment to the right breast had a lower quotient between the right side T_1 and the left side T_1 (p<0.05) whereas the two patients that received radiation treatment to the left side did not have a significantly different quotient. An analysis of pulmonary function tests in breast radiotherapy patients reveal a significant reduction in $D_{L,CO}$ and TLC persisting after 10 years [131]. Moreover, pulmonary perfusion defects can be linearly

predicted by the irradiated lung volume [132]. All of this indicates that T_1 is sensitive to late lung radiation damage and may reflect fibrosis and perfusion deficits.
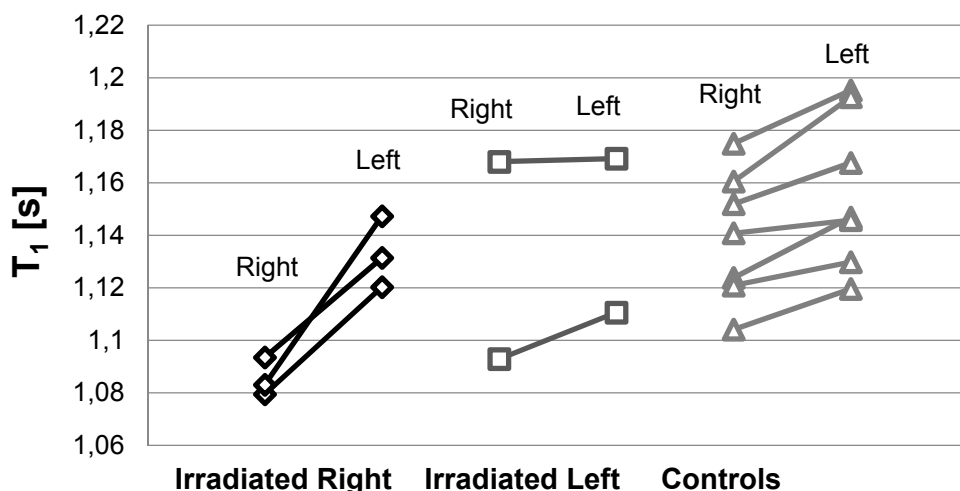
Figure 15 T_1 values in the left and right apical lung, 10 years after breast radiation treatment, compared to controls. The group that received treatment to the right breast had a significantly lower quotient T_1(right)/T_1(left) compared to controls (p<0.05). Presented at IWPFI, Edinburgh 2015 [129]

Although lower FEV_1 was related to decreased T_1 in COPD patients [125], it should be noted that this is because of the underlying disease –tissue destruction and loss of pulmonary blood. In 76 lung transplant patients with varying rejection symptoms (bronchiolitis obliterans), characterized by a reduction of FEV_1, no reduction of T_1 could be statistically detected (p=0.66) [133]. This indicates that obstructive airway disease does not necessarily affect pulmonary T_1, unless the underlying disease also results in tissue destruction or fibrosis, as in COPD and CF respectively.

9.6   Pulmonary T_1 and tobacco smoking

An interesting topic is whether tobacco smoking has an effect on T_1, if there is no underlying disease. In a group of 12 healthy smokers and 23 age matched non- smokers, there was a non-significant correlation between T_1 and pack-years when adjusted for age (p=0.08) and a significant correlation between T_1 and pack-years (p=0.02) after adjusting for age and height [134]. It is known that smoking has small effects on blood hematocrit and hemoglobin levels – in a Scandinavian reference population of 1800 people, smoking was associated with a 3.5 % increase in Hb and EVF in *females* but not men [68]. However, in a larger study of 6800 participants, no sex dependency was

reported and smoking more than 6 cigarettes per day was associated with both higher hematocrit and hemoglobin [69]. Still, a 3.5 % change in hematocrit or Hb would result in a change of similar magnitude in T_1 (approx. 40 ms) [20,70] which should not be detectable in a sample of 20 individuals. Moreover, pulmonary blood volume was not different between smokers and non-smokers when measured with PET [122]. Indeed, although $D_{L,CO}$ is reduced in smokers, the effective pulmonary capillary blood volume is only acutely reduced by inhaled CO [135,136]. Since the intrinsic T_1 of carboxyhemoglobin (CO-Hb) is the same as oxy-Hb [137] the reduction in $D_{L,CO}$ seen in smokers should not be relatable to T_1-endpoints in healthy smokers, as long as there is no underlying tissue destruction.

9.7 Pulmonary T_1 may or may not detect early damage caused by tobacco smoke

Inflammation is often used as a model for early smoking induced pulmonary damage and is visible as an increase in T_1 due to increased perfusion, edema and tissue cell infiltration. However, COPD contain a significant vasoconstrictive effect in the lung which induce – according to the previous paragraphs – a decrease in T_1. Thus, it is possible that the inflammatory and vasoconstrictive effects on T_1 oppose each other to yield a multi-phasic (or a net zero!) T_1 response to tobacco smoke induced lung damage:

Both T_1 and T_2 varies strongly with the water content of inflamed tissue, yielding a higher T_1 in the early inflammatory phase of a bleomycin challenge in mouse lungs [138–140]. Moreover, inflammation caused by endotoxin, protease and tobacco smoke induce V/Q mismatch in mice [141] and this perfusion mismatch is potentially brought about by an inhibition of hypoxic vasoconstriction in inflamed tissue [36,142] – yielding an additional perfusion induced increase of T_1.

However, the primary pathway for developing COPD may not be inflammation at all – but rather ischemia [143] – indeed, tobacco smoking is known to cause vasoconstriction and PAH [35,144]. The vasoconstriction is likely augmented by signal molecules such as leukotrienes [145,146] in response to irritants in the lung [4]. Pulmonary vasoconstriction may also be mediated by low oxygen saturation in the carotid bodies after smoking [13]. All of which decrease pulmonary blood and T_1.

The final caveat is nicotine itself, a powerful global vasoconstrictor acting through systemic and local catecholamine release [147] which promotes a low T_1 response to smoking. Moreover, nicotine interferes with vagus nerve *anti-inflammatory* pathways in lymphocytes through the nicotinic acetylcholine receptor (nAChR) [148–150], which may inhibit the inflammatory (T_1 up) aspect in early lung damage and tip the scales in favor of a T_1-reduction due to tobacco smoking

In conclusion, smoking induces both vasoconstriction (T_1 down) and inflammation (T_1 up) in the lung; there may be fast, transient and late effects; which are in turn mediated by oxygen tension, nicotine and a plethora of signal molecules. Needless to say, more studies are needed to elucidate the magnitudes and interactions of the inflammatory and vasoconstrictor responses on T_1 and the respective time courses.

10   Oxygen enhanced MRI

The oxygen enhancement effect was first studied in vivo and quantified as a relaxation enhancement of heart blood in 1984 [151] and the first proof of concept for OE-MRI of the lungs was provided in 1996 by Edelman et al. [8]. In 2002, Ohno et al. presented data that the mean relative enhancement ratio (MRER) in OE-MRI was correlated with $D_{L,CO}$ spurring the popularity of OE-MRI as a potential imaging method of regional lung function [9].

However, in **Paper 2** of this thesis work, in which $D_{L,CO}$ was compared to ΔR_1 in 30 healthy volunteers, no correlation could be found [77]. Instead the parameters that best explained the variation in the sample was BMI and age, with sex confounding, which can be understood in terms of pulmonary shunt [77]. The take home message is that in healthy individuals, the transfer of oxygen is not diffusion limited, as described in the physiology section, and OE-MRI will not correlate with $D_{L,CO}$. However, in disease it is still plausible that the OE-effect correlates with both T_1 and $D_{L,CO}$ because all are dependent on pulmonary blood volume.

10.1   The three-compartment model of ΔR_1

To describe the OE-effect as ΔR_1, the lung may be divided into four basic compartments: pulmonary arterial (non-oxygenated); pulmonary venous blood (oxygenated); pulmonary capillary blood (fully oxygenated after 1/3 at rest); and pulmonary tissue (**Paper 2**). In theory, the arterial oxygen partial pressure may rise from 90 mmHg to 600 mmHg in healthy individuals, including the effects of pulmonary shunt [29]. According to Silvennoinen [19] this will result in an arterial blood ΔR_1 of approximately 0.20 s^{-1} , which is considerably higher than observed (**Paper 2**). Moreover, measurements in bloodless porcine lungs indicate that the ΔR_1 in the lung tissue is on the order of 0.2 s^{-1} [118]. The only factor that can explain why ΔR_1 values in the range of 0.2 s^{-1} are not routinely observed is the presence of pulmonary arterial (non-oxygenated) blood. During oxygen breathing the pulmonary arterial oxygen content increase from 41 mmHg to 57 mmHg [152], resulting in a negative ΔR_1 of -0.5 s^{-1} [19]. The capillary blood is generally fully oxygenated after 1/3 of the capillary time, but may be considered to be *either* venous or arterial, but not both. This results

in a model where the expected ΔR_1 depends on the partitioning of blood as well as the tissue contribution, which we know from section 9.1 is echo-time dependent. A bold assumption of equal contributions from the post-capillary blood, pre-capillary blood, and tissue results in an expected change in relaxation rate of:

$$\Delta R_1 = \frac{\Delta R_{1,postc.} + \Delta R_{1,prec.} + \Delta R_{1,tissue}}{3} = \frac{0.2 s^{-1} - 0.05 s^{-1} + 0.2 s^{-1}}{3} = 0.117 s^{-1}$$

This is very much in line with the observed values in healthy volunteers (**paper 2**), the mean (standard deviation) sample value of a recent meta-analysis was 0.096 s^{-1} (0.025 s^{-1}) [93]. With these compartments in mind, a very effective way to change ΔR_1 is to change the blood volume, which is exactly what may happen in a diseased and chronic hypoxic lung exposed to 100% oxygen gas. The release of hypoxic pulmonary vasoconstriction may increase blood volume, which will increase T1; resulting in a negative ΔR_1 when the subject breathes 100% oxygen. The other major way to modulate ΔR_1 is by pulmonary shunt (Figure 2), which increases the fraction of non-oxygenated blood and lowers the oxygen content of the pulmonary venous system.

10.2   Methodological considerations for ΔR_1

In a recent meta-analysis, OE-measurements from 13 studies were pooled [93]. It is unfortunate that **Paper 2** was published the same year and was not included. The authors of the meta-study conclude that there is no systematic difference between spin-echo and gradient-echo sequences with respect to the oxygen enhancement effect, but this has not been established in a single cohort. In **paper 4** of this thesis we compared two IR-HASTE protocols with the classic Snapshot-FLASH and found that the mean T_1 and ΔR_1 are indeed different.

An important practical optimization is the choice of gas delivery. Although it was suggested that a loose fit, cheap face mask provides satisfactory oxygen enhancement compared to a tight fitting more expensive system [153], this was later refuted by another study, which claimed that the tight fitting mask system provided 50% higher oxygen enhancement at constant high oxygen flow [154]. Our own in-house tests confirm that a tight fitting mask is superior when studying oxygen enhancement, especially if the relaxation enhancement is quantified (Figure 16). In a clinical setting, a cheap loose-fit mask could potentially be used to generate images of e.g. pulmonary emboli and other perfusion defects in a non-quantitative manner.
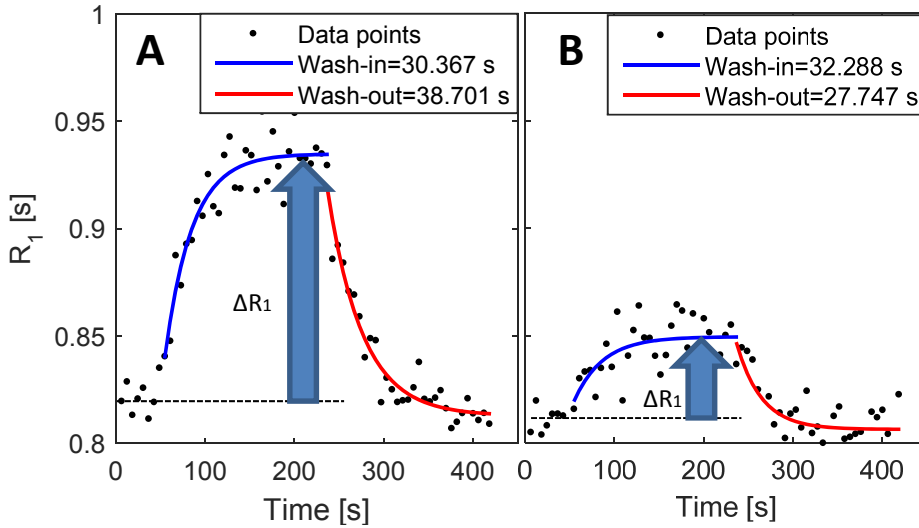
Figure 16 A: Example OE-MRI experiment in a healthy subject with a typical change in relaxation rate ΔR_1 of 0.12 s^{-1}, using a tight fitting face mask (Hans Rudolph V2-mask). B: the same subject with a conventional oxygen mask (Intersurgical). To get reliable results, a tight fitting mask must be used and oxygen equilibrium must be reached.

10.3 Oxygen enhanced MRI for Emphysema and COPD

The classic study by Ohno was made on a group of emphysema patients (n=10) and healthy controls (n=7) [9], where the oxygen signal enhancement was found to be lower in the emphysema group than the healthy controls. The same group of healthy volunteers were also compared to lung cancer patients with (n=8) and without emphysema(n=10) and signal enhancement was, as before, found to be lower patients with emphysema [155].

In another study, relaxation enhancement and oxygen wash-in time was measured in n=51 smokers with COPD, 10 smokers without COPD and 10 non-smokers, who also performed CT and PFT. All aspects of lung function: FEV_1, $D_{L,CO}$ and healthy lung tissue as seen on CT, correlated with both relaxation enhancement and wash-in time, as well as pack-years of cigarette use [156]. In the study, the wash-in time was more predictive of COPD severity classification than the relaxation enhancement.

A pharmacological trial used OE-MRI relaxation enhancement and wash-in/wash-out times as end-points when testing acute effects of a beta-2 agonist in 40 COPD patients (formoterol), as well as long term effects of a beta-2 agonist/corticosteroid treatment (formoterol/budesonide) [92]. The acute effects of beta-2 agonist inhalation was an

increase in FEV_1 and an increase in the wash-out time, however, only the increase in FEV_1 was statistically significant compared to placebo. The beta-2 agonist should relax airway smooth muscle within three minutes and the positive effects on heart rate and blood pressure should be on the order of 2 % (for 9 μg) and barely measureable within 3 hours [157]. The 8-week follow up revealed statistical significant increase in FEV_1, decrease in ΔR_1, and shortening of the wash-out time. The results must be interpreted with the non-oxygenated blood pool in mind, since the treatment may affect both shunting fraction and pulmonary vascular resistance.

10.4   Oxygen enhanced MRI in Cystic fibrosis

Cystic fibrosis is characterized by mucus plugging, distal airway inflammation and fibrosis, so it should be no surprise that the oxygen enhancement is severely reduced in afflicted lungs. In a group of 5 patients, the relaxation enhancement ΔR_1 in the CF lung was between 0 – 54 % of that of the normal lung [128].

In a more recent study, 21 CF patients and 5 volunteers were investigated with CT and OE-MRI with regional analysis based on 3 ROI per lung [10] . All regions of the lungs, except the basal third, exhibited a lower ΔR_1 in the CF patients compared to the healthy controls. Moreover, all regions of the lung – taken separately – had a longer wash-in time in the CF patients, whereas the whole lung wash-in time was not statistically different between healthy and CF subjects. The total wash-out time was longer in the CF lungs, but the variance was too large in the CF lungs to find statistical differences in all ROI. It is important to note that the heterogeneity in all end-points was larger in the CF patients.

In order to interpret such a study, with heterogeneous gas uptake and low enhancement regions, several physiological effects must be considered. For example, chronic hypoxic vasoconstriction in low ventilation areas may be alleviated by pulmonary *arterial* hyperoxia, which increases flow instantaneously. Upon return to normoxia, the hypoxic vasoconstriction is reactivated but at a slower rate (3-4 minutes) [13]. This interpretation is concurrent with the findings of the study, with the only caveat that pulmonary hypoxic vasoconstriction may be dependent on the alveolar oxygen tension and not be influenced by pulmonary arterial blood [34].

Finally, 6 CF patients and 5 asthmatics were compared to 7 healthy volunteers, using oxygen signal enhancement with a UTE-read out [158]. Considering the severe etiology of cystic fibrosis compared to asthma, it is not surprising that CF patients had lower signal enhancement than the asthma group. Moreover, the signal enhancement in the aorta was highest in the healthy volunteers and successively lower in asthma and CF.

10.5   Oxygen enhanced MRI correlates with asthma severity

Asthma is normally characterized by a considerable pulmonary shunt as outlined in the previous chapter. This means that a substantial fraction of the blood will pass the lung without being oxygenated, which may manifest as:

- The maximal oxygen concentration in efferent blood will be lower: ΔR_1 ↓

- The fraction of non-oxygenated blood will increase, where there is a negative oxygen enhancement effect: ΔR_1 ↓

- Since blood passes the lung without being oxygenated, more passes will be required to reach maximal oxygen concentration: **Wash-in time** ↑

In a study of 34 asthmatics, OE-MRI signal enhancement correlated with CT severity classification and with asthmatic stage classification [159]. In a smaller but more detailed study (4 mild, 6 severe) signal enhancement was found to be almost 50% lower in severe than mild asthma and heterogeneity worse in the severe condition [94], very coherent with the compromised ventilation/perfusion ratios in asthmatics [46]. The relaxation enhancement was also 30% lower in the aorta in the severe asthmatics, telling of a considerable shunt.

In a very elegant study ΔR_1 was quantified in asthmatics and control subjects exposed to several allergen challenges [160]. Despite being limited in size (9 asthmatics and 4 controls) the study found a significant transient reduction in oxygen enhancement after allergen challenge; in a dose dependent manner; where the decrease in ΔR_1 was proportional to the eosinophil infiltration (r= 0.67, P = .0001).

Pulmonary T_1 and ΔR_1 was quantified in 69 patients with transplanted lungs, with or without bronchitis obliterans syndrome (BOS) [133]. The typical manifestation is an immune mediated inflammation of the submucosa which ends in the obliteration of the airway by scar tissue formation [13]. The oxygen enhancement, quantified by ΔR_1, became lower with increasing symptom severity in the three groups stratified by FEV_1 >90%; 90% >FEV_1 >80%; and FEV_1 < 66%. This can be understood in the same terms as asthma, where airway obstruction leads to lower oxygen enhancement through pulmonary shunt.

It is important to remember that asthmatics often present with an elevated $D_{L,CO}$ [53–55] but evidently have very reduced ΔR_1. Thus, oxygen enhancement does not reflect pulmonary diffusion capacity, as was established in **Paper 2**.

10.6 Oxygen enhanced MRI and interstitial disease

Thin section CT and relaxation enhancement was used to distinguish patients with and without interstitial lung disease in a population with connective tissue disease (36 CTD of which 23 ILD) [161]. Both methods had comparable sensitivity but OE-MRI had very low specificity compared to CT (67 vs 100%), even though OE-MRI endpoints correlated marginally better with $D_{L,CO}$ (r=0.79 vs r=0.76) and serum ILD markers (KL-6; r=0.64 vs r=0.61) than disease severity assessed with thin-section CT. Interstitial lung disease is exactly the type of disease where oxygen transfer *is* diffusion limited, because the diffusion membrane thickness is increased, and OE-MRI may assess regional disease severity.

11   Pulmonary proton density

Structural pulmonary MRI has traditionally been hampered by the low proton density and air-tissue interfaces of the lung parenchyma, resulting in a very short T_2^*. However, with the advances in fast switching RF-transmitters and receivers; asymmetric echoes; non-Cartesian acquisition schemes; and faster iterative reconstruction algorithms, ultra-short echo time (UTE) imaging provides many interesting opportunities for pulmonary MRI.

11.1   MRI can be used to detect hyperintense or hypointense changes in the lung

In a mouse model of fibrosis the traditional FLASH and TSE as well as the novel UTE-sequence was able to detect both inflammation and fibrosis induces by bleomycin, although UTE-MRI was the modality that correlated best with CT [162]. Moreover, both FLASH and UTE can be effectively used to detect pulmonary nodules in humans, however, UTE has a 80% detection rate at >6 mm nodules, whereas FLASH has a 80% detection rate at 10 mm nodules [163].

Overall, MRI and especially UTE, has a large potential to study a variety of pathological changes. In a group of 85 patients with a plethora of clinical manifestations, the kappa statistic for inter-measurement agreement was between 0.67 and 0.99, indicating an often near perfect agreement between standard dose CT, low-dose CT and UTE-MRI [164]. Another study was limited to 30 cystic fibrosis patients and also found an inter-measurement kappa value of >0.8 for pathologic changes between UTE-MRI and CT [165] – this was true for all findings except emphysema, for which kappa = 0.44.

The introduction of UTE has spurred the interest in MRI also for hypointense changes such as emphysema. In a rat emphysema model, UTE signal correlated well with CT attenuation values (R=0.88) [166]. A similar result was found in a group of COPD subjects and healthy controls, where the correlation between CT attenuation and UTE signal was r=0.82-0.99 [167]. However, it must be stressed that this UTE-scan was made with 1.5 cm slice thickness and that the acquisition time was 13 seconds of breath-hold per slice.

11.2 Quantitative MRI proton density can potentially be used to detect emphysema

Although the use of CT-similar contrast may be clinically useful – especially for pediatric applications or repeated measures – the huge variety in MRI settings makes intra patient comparison difficult. For this reason quantitative signal mapping can be used. By generating proton density maps; minimizing the influence of T_1 and T_2^* relaxation; and normalizing the signal intensity to a known tissue, the signal will reflect the tissue density.

In a group of 24 COPD patients and 12 volunteers, an IR-HASTE protocol was used to generate proton density maps (under the assumption that PD=equilibrium signal). By calculating established quantitative CT end-points (density mask [168]) from the PD-images, quantitative proton density MRI was thus enabled [169]. This type of quantitative density MRI protocol had been previously used with a HASTE sequence. As part of **Paper 3**, this method was adapted to the Snapshot-FLASH and tested against the AiDA-airspace radius. As expected, all measures of quantitative proton density correlated with the estimated airspace radius, where a low density was associated with a large airspace radius.
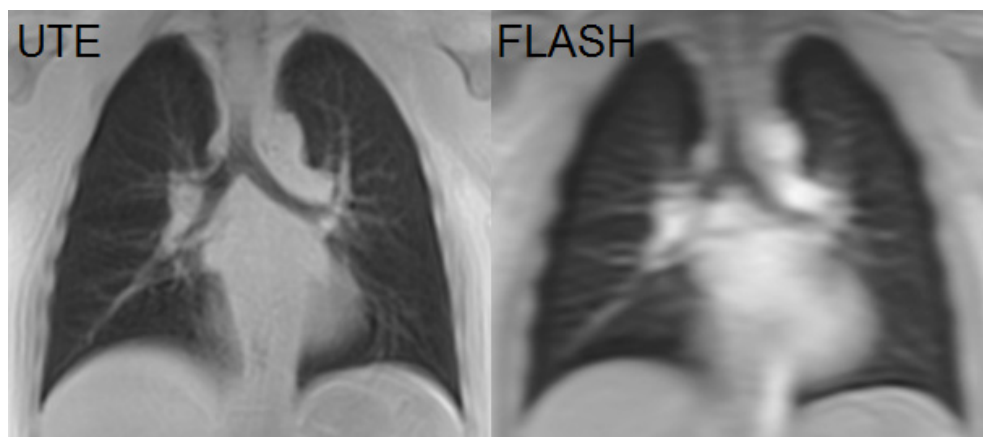
Figure 17 LEFT: PD weighted UTE-image of healthy lungs. The short echo time allows signal to be generated in distal airway blood vessels and with sufficient resolution, almost CT-identical images can be formed. RIGHT: snapshot FLASH PD-map of the same subject. The resolution is not comparable to the UTE-image, but there is signal from the whole lung. This image can be used for quantitative mapping, but not as a clinical image.

12   Discussion

12.1   Major findings

The major findings in this thesis are the following:

- Pulmonary T_1 is age and sex dependent where young females have a significantly higher T_1. This can likely be explained in terms of pulmonary blood and residual volume.

- The oxygen enhancement effect as quantified by ΔR_1 is not correlated with $D_{L,CO}$ in a healthy population. This does not contradict the previous reported correlation between oxygen signal enhancement and $D_{L,CO}$. It is, on the contrary, very likely that ΔR_1 correlates with most measures of pulmonary function in advanced pulmonary disease.

- The oxygen enhancement effect as quantified by ΔR_1 is dependent on age and BMI in a healthy population. This is likely an effect of pulmonary shunting, where excess adipose tissue restricts the lung volume and produces non-ventilated areas. High age is also known to reduce the lung compliance and thus increase the shunt fraction.

- Most quantitative OE-MRI protocols can be combined with a pulmonary proton density measurement without any additional scanning time. The M_0- maps produced by the Snapshot-FLASH sequence does correlate with distal airspace radius measured with AIDA – this is valuable complementary information that has previously been overlooked.

- Different measurement protocols will produce different results, both with respect to native T_1 and the OE-effect. Of particular importance is the difference between gradient echo and spin echo based quantifications and the use of selective or global inversion pulses.

The above findings can mostly be appreciated as an imperative to include a physiological model based on pulmonary perfusion in all OE-MRI research. Previous research has been too reliant on pathological models of diffusion [92], which are not generalizable to all patient groups and definitely not healthy volunteers. Moreover, one of the primary components of the OE-effect is pulmonary shunt fraction, which varies

with age, sex and BMI. The field of MRI is a truly cross disciplinary, where the determinants of the MRI signal are distributed between purely physical (flip angle and protocol) and purely biological (macromolecule and blood flow) parameters. Any attempt to describe the MRI signal must thus be equally physical and biological in nature.

Oxygen enhanced MRI does not only provide a means of measuring $D_{L,CO}$ in severe disease – if used with caution it has the potential to identify regions with pulmonary shunt, precapillary hypertension and interstitial disease. Asthma and cystic fibrosis are some of the diseases where severity correlate well with OE-endpoints. Finally, OE-MRI may easily be accompanied by a proton density quantification to detect emphysema.

12.2 Research context

According to this thesis, oxygen enhanced MRI is not ready to be used for diagnostic purposes, but has substantial potential for tracking and phenotyping disease. The largest studies have included less than 100 patients with of a single disease type and the ROC-analysis of OE-MRI have not produced an AUC larger than 0.8 [133,169]. Even if the results were impressive, the variability of end-points and methodology makes any generalization difficult.

A completely different application of OE-MRI is for tumor hypoxia tracking, which has not been covered in this thesis. Tumor oxygen consumption, outside the lung, can be studied by the same principles as in pulmonary OE-MRI [170]. This technique greatly increases the clinical usefulness of OE-MRI since the same modality can be used to track tumor growth and pulmonary function.

12.3 Limitations

Most MRI studies suffer from a low number of subjects and measurements. The time and cost of MRI examinations are at least twice that of corresponding CT-examination and the clinical availability of scanners is very restricted. This thesis contains the, up to this date, largest cohort of healthy volunteers with T_1 and OE-measurements, but it is still only 31 subjects.

Another important limitation of this thesis is the lack of patients and pathology. There are many ideas in this thesis that may be tested on a suitable group of patients or animal models. This, however, is promising for the future of OE-MRI.

This thesis has an emphasis on pulmonary blood for OE-MRI interpretation – therefore it is regrettable that no proper blood work was done on the original cohort that was later used in papers 1-3. It is recommended that any future study of OE-MRI should include measurements of hemoglobin and/or hematocrit, at least.

Another limitation is the choice to perform our measurements during tidal inspiration. Previous T_1-measurements have established a significant difference between respiratory phases [121], thus, the most informative protocol, with respect to disease phenotyping, would include measurements at both inspiration and expiration [130]. An interesting option is the Fourier decomposition technique that has been used to study respiratory motion on a pixel-by-pixel level during free breathing [171,172].

12.4 Methodology

All papers published in this thesis contain multiple comparisons. It is my firm belief that p-values should not be "adjusted" in this type of methodological works. For example, the fact that the T_1-values correlate with all lung volumes for males should not be surprising – since all lung volumes do correlate with each other and we do know that T_1 should vary with lung volume. It is way more dangerous to report only significant correlations and to refrain from publishing results because they did not fit the original model or the specified significance levels. In **paper 2** for example, the data were turned inside out because the reported correlation between $D_{L,CO}$ and ΔR_1 could not be seen. This instead led to an alternative physiological explanation for the OE-effect, along with a physiological model that gave a much better fit to the data.

12.5 Future prospects

The availability of UTE-protocols and the addition of the Snapshot-FLASH to the commercial package of clinical scanners have changed the arena for OE-MRI and pulmonary MRI in general. The CT-imitating potential of UTE sequences makes pulmonary MRI clinically useful and oxygen enhanced MRI with breath-holding can easily be performed by any center, without post-processing.

Cardiac output would also be interesting study together with OE-parameters. Given that Look-Locker derived protocols are used to study myocardial T_1 [74], a cardiopulmonary OE-protocol is feasible, although time-consuming. Extending 3D-cardiac MRI to the whole thorax and implementing a UTE read-out, would invite to a holistic cardiopulmonary scan with OE-potential and simultaneous quantification of

pulmonary tissue density and myocardial T_1. Studying the cardiopulmonary system as one unit may be very valuable for COPD/PAH phenotype [58].

The PAH patient, may be an illustrative model for the negative ΔR_1 effect, predicted by the compartment model of ΔR_1 in section 10.1. A patient with PAH will exhibit vessel distention in the pulmonary arterial side [59], which should yield a negative ΔR_1 in an OE-experiment. Moreover, breathing oxygen gas may alleviate pulmonary hypoxic vasoconstriction, leading to an increase in pulmonary blood volume and a further increase in T_1 (negative ΔR_1). Cardiac MRI has already been used to study PAH in a systemic sclerosis population compared to controls, with very meagre results [173]. It is possible that OE-MRI will provide a very sensitive screening tool for PAH, by directly imaging the pulmonary arterial blood compartment.

As outlined in section 9.7, the etiology of COPD may be both inflammatory and ischemic [143]. Potentially, nicotine is a key player with anti-inflammatory and vasoconstrictive effects [174,175]. The OE and T1 biomarkers presented in this thesis may be a tool to elucidate the vasoconstrictor and inflammatory effects of tobacco smoke, and nicotine alone, *in vivo*, in both healthy smokers and animal models.

The effects of oxygen inhalation on T_2^* and susceptibility differences between the pulmonary arterial, venous and capillary blood pools is only briefly mentioned in section 5.3. Any method that can selectively image each of these components will be immensely valuable for disease phenotyping. A possible starting point is single point spectroscopy under oxygen breathing with susceptibility modelling [65].

This thesis contains the first coherent report of the OE-effect from the bench to the bedside (or from atom to asthma). A significant effort was made to connect the work on molecular imaging using oxygen NMR [97,104], with the macroscopic relaxation effects, but this could not be done in a quantitative manner. The first step is to quantify the relaxivity of oxygen in different protein solutions, to yield a concentration dependent relaxivity of oxygen in hemoglobin and albumin. Another interesting task is to quantify the relaxivity of oxygen in different cell concentrations – indeed, the relaxivity is known to vary with hematocrit, which may prove to be an effect of the amount of cells and not the amount of hemoglobin, since oxygen is non-polar and preferentially occupies cell walls [101].

Paper 4 provides the first evidence that spin-echo and gradient-echo quantifications of ΔR_1 do not yield the same results. This is certainly an invitation to anyone to replicate or challenge these results. The hypothesis put forward in this thesis emphasizes the peri-alveolar water, including surfactant and alveolar capillaries, which potentially have the highest oxygen concentrations and the highest susceptibility gradients. A carefully designed experiment may investigate whether this peri-alveolar water pool contributes with a large ΔR_1 in spin-echoes, but not in gradient echoes due to excessive T_2^* dephasing.

12.6   Conclusions

- In this thesis you will find a careful description of the variation in T_1 and ΔR_1 in a cohort of healthy volunteers (Paper 1 & 2). A recent meta-analysis confirm that the values presented here are coherent with other studies [93].

- The body of this thesis contains a thorough physiological and physical interpretation of pulmonary T_1 and ΔR_1 that incorporates other studies on pathology (Chapters 2 through 10)

- In paper 3, there is evidence that the common Snapshot FLASH sequence for T_1-quantification provides additional biomarkers for lung density, as the equilibrium signal $\mathbf{M_0}$. Considering the usefulness of this biomarker alone (Chapter 11), OE-MRI with T_1- and PD-mapping will be a very useful imaging tool.

- Paper 4 provide evidence that gradient echoes and spin echoes may produce different results with respect to T_1 and ΔR_1 This is supported in section 9.2 with data from a meta-analysis.

- As a whole, this thesis can be used by anyone wishing to start an OE-MRI pipeline or study. Hopefully, there will be plenty of information and suggestions for further investigations. The references contain a mix of MRI physics, basic pulmonary physiology and state-of-the-art clinical applications of pulmonary OE-MRI, which provides a sound foundation of any aspiring OE-MRI researcher.

These conclusions warrant a more careful interpretation of pulmonary T_1 and oxygen induced ΔR_1, where pulmonary blood and shunting should be included. Neither T_1 or ΔR_1 should be seen as intrinsic parameters, but are dependent on both very physiochemical processes, such as oxygen-protein relaxation interactions; macroscopic biology, such as blood flow; and MRI sequence design.

A more optimistic implication of this thesis is that oxygen induced ΔR_1 and T_1 are imaging biomarkers, sensitive enough to detect differences brought about by natural ageing, weight gain and sex differences in pulmonary physiology. This should make OE-MRI and pulmonary T_1-quantification ideal for detecting disease. Indeed, most pathological changes will have an effect on both T_1 and ΔR_1 in the lung – the only question is how (spin- or gradient-echo), when (respiratory phase) and where (pulmonary arterial, capillary or venous compartment) you choose to measure.

13 References

1. WHO. WHO Top 10 causes of death [Internet]. World Health Organization; 2018 [cited 4 Jul 2018]. Available: http://www.who.int/gho/mortality_burden_disease/causes_death/top_10/en/

2. Burney PGJ, Patel J, Newson R, Minelli C, Naghavi M. Global and regional trends in COPD mortality, 1990-2010. Eur Respir J. European Respiratory Society; 2015;45: 1239–47. doi:10.1183/09031936.00142414

3. Kilic H, Kokturk N, Sari G, Cakır M. Do females behave differently in COPD exacerbation? Int J Chron Obstruct Pulmon Dis. Dove Press; 2015;10: 823–30. doi:10.2147/COPD.S78952

4. West JB. Respiratory Physiology: The Essentials [Internet]. 9:th Editi. Baltimore: Lippincott Williams & Wilkins; 2012. Available: https://books.google.ca/books/about/Respiratory_Physiology.html?id=rHaZVmFZRVcC&pgis=1

5. Vogelmeier CF, Criner GJ, Martinez FJ, Anzueto A, Barnes PJ, Bourbeau J, et al. Global Strategy for the Diagnosis, Management, and Prevention of Chronic Obstructive Lung Disease 2017 Report. GOLD Executive Summary. Am J Respir Crit Care Med. 2017;195: 557–582. doi:10.1164/rccm.201701-0218PP

6. van Mens TE, Scheres LJ, de Jong PG, Leeflang MM, Nijkeuter M, Middeldorp S. Imaging for the exclusion of pulmonary embolism in pregnancy. Cochrane Database Syst Rev. 2017;1: CD011053. doi:10.1002/14651858.CD011053.pub2

7. Chiarotti G, Cristiani G, Giulotto L. Proton relaxation in pure liquids and in liquids containing paramagnetic gases in solution. Nuovo Cim. Società Italiana di Fisica; 1955;1: 863–873. doi:10.1007/BF02731333

8. Edelman RR, Hatabu H, Tadamura E, Li W, Prasad P V. Noninvasive Assessment of Regional ventilation in the human lung using oxygen-enhanced magnetic resonance imaging. Nat Med. 1996;2: 1236–1239.

9. Ohno Y, Hatabu H, Takenaka D, Van Cauteren M, Fujii M, Sugimura K. Dynamic oxygen-enhanced MRI reflects diffusing capacity of the lung. Magn Reson Med. 2002;47: 1139–44. doi:10.1002/mrm.10168

10. Martini K, Gygax CM, Benden C, Morgan AR, Parker GJM, Frauenfelder T. Volumetric dynamic oxygen-enhanced MRI (OE-MRI): comparison with CT Brody score and lung function in cystic fibrosis patients. Eur Radiol. European Radiology; 2018; 1–11. doi:10.1007/s00330-018-5383-5

11. Kershaw LE, Naish JH, McGrath DM, Waterton JC, Parker GJM. Measurement of arterial plasma oxygenation in dynamic oxygen-enhanced MRI. Magn Reson Med. 2010;64: 1838–42. doi:10.1002/mrm.22571

12. Zaharchuk G, Busse RF, Rosenthal G, Manley GT, Glenn O a., Dillon WP. Noninvasive Oxygen Partial Pressure Measurement of Human Body Fluids In Vivo Using Magnetic Resonance Imaging. Acad Radiol. 2006;13: 1016–1024. doi:10.1016/j.acra.2006.04.016

13. Crystal RG, West JB, Barnes PJ, Weibel ER. The Lung: Scientific Foundations. 2nd ed. Philadelphia: Lippincott-Raven; 1997.

14. Ley S, Puderbach M, Risse F, Ley-Zaporozhan J, Eichinger M, Takenaka D, et al. Impact of oxygen inhalation on the pulmonary circulation: assessment by magnetic resonance (MR)-perfusion and MR-flow measurements. Invest Radiol. 2007;42: 283–290. doi:10.1097/01.rli.0000258655.58753.5d\n00004424-200705000-00003 [pii]

15. Glick G, Schreiner BF, Murphy GW, Yu PN. Effects of Inhalation of 100 Per Cent Oxygen on the Pulmonary Blood Volume in Patients with Organic Heart Disease. Circulation. 1963;27: 541–553. doi:10.1161/01.CIR.27.4.541

16. Stanisz GJ, Henkelman RM. Gd-DTPA relaxivity depends on macromolecular content. Magn Reson Med. 2000;44: 665–667. doi:10.1002/1522-2594(200011)44:5<665::AID-MRM1>3.0.CO;2-M

17. Zheng S, Xia Y. The impact of the relaxivity definition on the quantitative measurement of glycosaminoglycans in cartilage by the MRI dGEMRIC method. Magn Reson Med. 2010;63: 25–32. doi:10.1002/mrm.22169

18. Köylü MZ, Asubay S, Yilmaz A. Determination of proton relaxivities of Mn(II), Cu(II) and Cr(III) added to solutions of serum proteins. Molecules. 2009;14: 1537–45. doi:10.3390/molecules14041537

19. Silvennoinen MJ, Kettunen MI, Kauppinen R a. Effects of hematocrit and oxygen saturation level on blood spin-lattice relaxation. Magn Reson Med. 2003;49: 568–571. doi:10.1002/mrm.10370

20. Spees WMW, Yablonskiy DA Da, Oswood MC, Ackerman JJH. Water proton MR properties of human blood at 1.5 Tesla: Magnetic susceptibility, T1, T2, T2*, and non Lorentzian signal behavior. Magn Reson …. 2001;45: 533–542. doi:10.1002/mrm.1072

21.   Quanjer PH, Tammeling GJ, Cotes JE, Pedersen OF, Peslin R, Yernault JC. Lung volumes and forced ventilatory flows. Report Working Party Standardization of Lung Function Tests, European Community for Steel and Coal. Official Statement of the European Respiratory Society. Eur Respir J Suppl. 1993;16: 5–40. Available: http://www.ncbi.nlm.nih.gov/pubmed/8499054

22.   Powers SK, Lawler J, Dempsey JA, Dodd S, Landry G. Effects of incomplete pulmonary gas exchange on VO2 max. J Appl Physiol. 1989;66: 2491–2495. doi:10.1152/jappl.1989.66.6.2491

23.   Molina DK, Dimaio VJM. Normal organ weights in men: Part II-the brain, lungs, liver, spleen, and kidneys. Am J Forensic Med Pathol. 2012;33: 368–372. doi:10.1097/PAF.0b013e31823d29ad

24.   Aggarwal S, Gross CM, Porcelli RJ, Black SM. Pulmonary Hemodynamics [Internet]. Second Edi. Comparative Biology of the Normal Lung. Elsevier Inc.; 2015. doi:10.1016/B978-0-12-404577-4.00014-X

25.   Janssens JP, Pache JC, Nicod LP. Physiological changes in respiratory function associated with ageing. Eur Respir J. 1999;13: 197–205. Available: http://www.ncbi.nlm.nih.gov/pubmed/10836348

26.   Verbeken EK, Cauberghs M, Mertens I, Clement J, Lauweryns JM, Van de Woestijne KP. The senile lung; Comparison with normal and emphysematous lungs. 2. Functional aspects. Chest. 1992;101: 800–809. doi:10.1378/chest.101.3.793

27.   Stocks J, Quanjer PH. Reference values for residual volume, functional residual capacity and total lung capacity: ATS Workshop on Lung Volume Measurements Official Statement of the European Respiratory Society. Eur Respir J. 1995;8: 492–506. doi:10.1183/09031936.95.08030492

28.   Eroschenko VP, Fiore MSH di. DiFiore's atlas of histology with functional correlations [Internet]. Wolters Kluwer Health/Lippincott Williams & Wilkins; 2013. Available: https://books.google.se/books/about/DiFiore_s_Atlas_of_Histology_with_Functi.html?id=sH87M12QswcC&redir_esc=y

29.   Harris EA, Seelye ER, Whitlock RM. Revised standards for normal resting dead-space volume and venous admixture in men and women. Clin Sci Mol Med. 1978;55: 125–8. Available: http://www.ncbi.nlm.nih.gov/pubmed/668265

30.   Jones RL, Nzekwu MM. The effects of body mass index on lung volumes. Chest. The American College of Chest Physicians; 2006;130: 827–833. doi:10.1378/chest.130.3.827

31.   O'Donnell DE, O'Donnell CDJ, Webb KA, Guenette JA. Respiratory consequences of mild-to-moderate obesity: Impact on exercise performance in health and in chronic obstructive pulmonary disease. Pulm Med. 2012;2012. doi:10.1155/2012/818925

32. Jensen RL, Crapo RO. Prediction of normal arterial oxygen levels. J Investig Med. 1996;44. Available: http://www.scopus.com/inward/record.url?eid=2-s2.0-33749579700&partnerID=tZOtx3y1

33. Jenkins SC, Moxham J. The effects of mild obesity on lung function. Respir Med. 1991;85: 309–11. Available: http://www.ncbi.nlm.nih.gov/pubmed/1947368

34. Wang L, Yin J, Nickles HT, Ranke H, Tabuchi A, Hoffmann J, et al. Hypoxic pulmonary vasoconstriction requires connexin 40-mediated endothelial signal conduction. J Clin Invest. American Society for Clinical Investigation; 2012;122: 4218–4230. doi:10.1172/JCI59176

35. Chaouat a, Chaouat a, Naeije R, Naeije R, Weitzenblum E, Weitzenblum E. Pulmonary hypertension in COPD. Eur Respir J Off J Eur Soc Clin Respir Physiol. 2008;32: 1371–85. doi:10.1183/09031936.00015608

36. Hoffman EA. State of the Art. A Structural and Functional Assessment of the Lung via Multidetector-Row Computed Tomography: Phenotyping Chronic Obstructive Pulmonary Disease. Proc Am Thorac Soc. 2006;3: 519–532. doi:10.1513/pats.200603-086MS

37. Toren K, Olin A-C, Lindberg A, Vikgren J, Brandberg J, Johnsson Å, et al. Vital capacity and COPD: the Swedish CArdioPulmonary bioImage Study (SCAPIS). Int J Chron Obstruct Pulmon Dis. Dove Press; 2016;11: 927. doi:10.2147/COPD.S104644

38. Wang W, Ma D, Li T, Ying Y, Xiao W. People with older age and lower FEV1%pred tend to have a smaller FVC than VC in pre-bronchodilator spirometry. Respir Physiol Neurobiol. 2014;194: 1–5. doi:10.1016/j.resp.2014.01.003

39. Yuan W, He X, Xu Q-F, Wang H-Y, Casaburi R. Increased difference between slow and forced vital capacity is associated with reduced exercise tolerance in COPD patients. BMC Pulm Med. 2014;14: 16. doi:10.1186/1471-2466-14-16

40. Cotes JE, Chinn DJ, Quanjer PH, Roca J, Yernault JC. Standardization of the measurement of transfer factor (diffusing capacity). Report Working Party Standardization of Lung Function Tests, European Community for Steel and Coal. Official Statement of the European Respiratory Society. Eur Respir J Suppl. 1993;16: 41–52. Available: http://www.ncbi.nlm.nih.gov/pubmed/8499053

41. Piirilä P, Seikkula T, Välimäki P. Differences between Finnish and European reference values for pulmonary diffusing capacity. Int J Circumpolar Health. 2007;66: 449–457. doi:10.3402/ijch.v66i5.18316

42. Jakobsson JKF, Hedlund J, Kumlin J, Wollmer P, Löndahl J. A new method for measuring lung deposition efficiency of airborne nanoparticles in a single breath. Sci Rep. Nature Publishing Group; 2016;6: 36147. doi:10.1038/srep36147

43. Löndahl J, Jakobsson JKF, Broday DM, Aaltonen HL, Wollmer P. Do nanoparticles provide a new opportunity for diagnosis of distal airspace disease? Int J Nanomedicine. Dove Press; 2017;12: 41–51. doi:10.2147/IJN.S121369

44.   Aaltonen HL, Jakobsson JK, Diaz S, Zackrisson S, Piitulainen E, Löndahl J, et al. Deposition of inhaled nanoparticles is reduced in subjects with COPD and correlates with the extent of emphysema: Proof of concept for a novel diagnostic technique. Clin Physiol Funct Imaging. 2018; 1008–1014. doi:10.1111/cpf.12517

45.   Jakobsson JKF, Aaltonen HL, Nicklasson H, Gudmundsson A, Rissler J, Wollmer P, et al. Altered deposition of inhaled nanoparticles in subjects with chronic obstructive pulmonary disease. BMC Pulm Med. BMC Pulmonary Medicine; 2018;18: 129. doi:10.1186/s12890-018-0697-2

46.   West JB. Pulmonary Pathophysiology: The Essentials [Internet]. 2011. Available: https://books.google.se/books/about/Pulmonary_Pathophysiology.html?id=slJg1I9N CuIC&pgis=1

47.   Stoller JK, Aboussouan LS. Alpha1-antitrypsin deficiency. Lancet (London, England). 2005;365: 2225–36. doi:10.1016/S0140-6736(05)66781-5

48.   Rennard SI, Vestbo J. COPD: the dangerous underestimate of 15%. Lancet. Elsevier; 2006;367: 1216–1219. doi:10.1016/S0140-6736(06)68516-4

49.   Barnes PJ. Inflammatory mechanisms in patients with chronic obstructive pulmonary disease. J Allergy Clin Immunol. 2016;138: 16–27. doi:10.1016/j.jaci.2016.05.011

50.   Domej W, Oettl K, Renner W. Oxidative stress and free radicals in COPD--implications and relevance for treatment. Int J Chron Obstruct Pulmon Dis. 2014;9: 1207–24. doi:10.2147/COPD.S51226

51.   STOCKLEY RA. Neutrophils and Protease/Antiprotease Imbalance. Am J Respir Crit Care Med. 1999;160: S49–S52. doi:10.1164/ajrccm.160.supplement_1.13

52.   Tunsäter A. Astma, vuxna - utredning och behandling [Internet]. internetmedicin.se; 2017 [cited 22 Aug 2018]. Available: https://www.internetmedicin.se/page.aspx?id=230

53.   Weitzman RH, Wilson AF. Diffusing capacity and over-all ventilation: Perfusion in asthma. Am J Med. Elsevier; 1974;57: 767–774. doi:10.1016/0002-9343(74)90851-1

54.   Saydain G, Beck KC, Decker PA, Cowl CT, Scanlon PD. Clinical significance of elevated diffusing capacity. Chest. 2004;125: 446–52. Available: http://www.ncbi.nlm.nih.gov/pubmed/14769723

55.   Collard P, Njinou B, Nejadnik B, Keyeux A, Frans A. Single breath diffusing capacity for carbon monoxide in stable asthma. Chest. 1994;105: 1426–9. Available: http://www.ncbi.nlm.nih.gov/pubmed/8181330

56.   GINA. Global Strategy for Asthma Management and Prevention [Internet]. Global Initiative for Asthma. 2018. Available: https://ginasthma.org/

57.   Ulrich M, Worlitzsch D, Viglio S, Siegmann N, Iadarola P, Shute JK, et al. Alveolar inflammation in cystic fibrosis. J Cyst Fibros. 2010;9: 217–227. doi:10.1016/j.jcf.2010.03.001

58.   Shujaat A, Bajwa AA, Cury JD. Pulmonary hypertension secondary to COPD. Pulm Med. 2012;2012. doi:10.1155/2012/203952

59.   Barberà JA, Peinado VI, Santos S. Pulmonary hypertension in chronic obstructive pulmonary disease. Eur Respir J. 2003;21: 892–905. doi:10.1183/09031936.03.00115402

60.   Olsson LE, Lindahl M, Önnervik PO, Johansson LB, Palmér M, Reimer MK, et al. Measurement of MR signal and T2* in lung to characterize a tight skin mouse model of emphysema using single-point imaging. J Magn Reson Imaging. 2007;25: 488–494. doi:10.1002/jmri.20840

61.   Triphan SMF, Breuer FA, Gensler D, Kauczor H-U, Jakob PM. Oxygen enhanced lung MRI by simultaneous measurement of T1 and T2 * during free breathing using ultrashort TE. J Magn Reson Imaging. 2014;41: 1708–14. doi:10.1002/jmri.24692

62.   Arnold JFT, Fidler F, Wang T, Pracht ED, Schmidt M, Jakob PM. Imaging lung function using rapid dynamic acquisition of T1-maps during oxygen enhancement. MAGMA. 2004;16: 246–53. doi:10.1007/s10334-004-0034-z

63.   Duyn JH. Steady state effects in fast gradient echo magnetic resonance imaging. Magn Reson Med. 1997;37: 559–68. Available: http://www.ncbi.nlm.nih.gov/pubmed/9094078

64.   Hatabu H, Alsop DC, Listerud J, Bonnet M, Gefter WB. T2* and proton density measurement of normal human lung parenchyma using submillisecond echo time gradient echo magnetic resonance imaging. Eur J Radiol. 1999;29: 245–52. Available: http://www.ncbi.nlm.nih.gov/pubmed/10399610

65.   Mulkern R V., Haker S, Hatsuho M, Lee E, Mitsouras D, Oshio K, et al. Lung Parenchymal Signal Intensity in MRI: A Technical Review with Educational Aspirations Regarding Reversible Versus Irreversible Transverse Relaxation Effects in Common Pulse Sequences. Concepts Magn Reson Part A Bridg Educ Res. 2014;43: 29–53. doi:10.1002/cmr.a.21297

66.   Cooper MA, Nguyen TD, Spincemaille P, Prince MR, Weinsaft JW, Wang Y. How accurate is MOLLI T1 mapping in vivo? Validation by spin echo methods. PLoS One. 2014;9: e107327. doi:10.1371/journal.pone.0107327

67.   Ittermann T, Roser M, Wood G, Preez H, Lüdemann J, Völzke H, et al. Reference intervals for eight measurands of the blood count in a large population based study. Clin Lab. 2010;56: 9–19. Available: http://www.scopus.com/inward/record.url?eid=2-s2.0-77950258725&partnerID=tZOtx3y1

68.   Nordin G, Mårtensson a, Swolin B, Sandberg S, Christensen NJ, Thorsteinsson V, et al. A multicentre study of reference intervals for haemoglobin, basic blood cell counts and erythrocyte indices in the adult population of the Nordic countries. Scand J Clin Lab Invest. 2004;64: 385–398. doi:10.1080/00365510410002797

69. Eisenga MF, Kieneker LM, Touw DJ, Nolte IM, van der Meer P, Huls G, et al. Active Smoking and Hematocrit and Fasting Circulating Erythropoietin Concentrations in the General Population. Mayo Clin Proc. Mayo Foundation for Medical Education and Research; 2018;93: 337–343. doi:10.1016/j.mayocp.2018.01.005

70. Li W, Grgac K, Huang A, Yadav N, Qin Q, van Zijl PCMM. Quantitative theory for the longitudinal relaxation time of blood water. Magn Reson Med. 2015;00: n/a-n/a. doi:10.1002/mrm.25875

71. Blockley NP, Jiang L, Gardener a. G, Ludman CN, Francis ST, Gowland P a. Field strength dependence of R_1 and R2* relaxivities of human whole blood to prohance, vasovist, and deoxyhemoglobin. Magn Reson Med. 2008;60: 1313–1320. doi:10.1002/mrm.21792

72. Brahm J. The permeability of red blood cells to chloride, urea and water. J Exp Biol. 2013;216: 2238–2246. doi:10.1242/jeb.077941

73. Gianolio E, Ferrauto G, Di Gregorio E, Aime S. Re-evaluation of the water exchange lifetime value across red blood cell membrane. Biochim Biophys Acta - Biomembr. Elsevier; 2016;1858: 627–631. doi:10.1016/J.BBAMEM.2015.12.029

74. Piechnik SK, Ferreira VM, Lewandowski AJ, Ntusi NAB, Banerjee R, Holloway C, et al. Normal variation of magnetic resonance T1 relaxation times in the human population at 1.5 T using ShMOLLI. J Cardiovasc Magn Reson. 2013;15: 13. doi:10.1186/1532-429X-15-13

75. Nilsson-Ehle P, Berggren Söderlund M, Theodorsson E, Becker C, Grankvist K. Laurells Klinisk Kemi i praktisk medicin. 9th ed. Grubb A, editor. Studentlitteratur; 2011.

76. Rehman HU. Methemoglobinemia. West J Med. BMJ Publishing Group; 2001;175: 193–6. Available: http://www.ncbi.nlm.nih.gov/pubmed/11527852

77. Kindvall SSISSI, Diaz S, Svensson J, Wollmer P, Olsson LELE. The change of longitudinal relaxation rate in oxygen enhanced pulmonary MRI depends on age and BMI but not diffusing capacity of carbon monoxide in healthy never-smokers. PLoS One. 2017;12: e0177670. doi:10.1371/journal.pone.0177670

78. Maxien D, Dietrich O, Thieme SF, Förster S, Behr J, Reiser MF, et al. Value of oxygen-enhanced MRI of the lungs in patients with pulmonary hypertension: a qualitative and quantitative approach. J Magn Reson Imaging. 2012;35: 86–94. doi:10.1002/jmri.22740

79. Weaving G, Batstone GF, Jones RG. Age and sex variation in serum albumin concentration: an observational study. Ann Clin Biochem An Int J Biochem Lab Med. 2015;0: 1–6. doi:10.1177/0004563215593561

80. Gonzalez-Quintela A, Alende R, Gude F, Campos J, Rey J, Meijide LM, et al. Serum levels of immunoglobulins (IgG, IgA, IgM) in a general adult population and their relationship with alcohol consumption, smoking and common metabolic abnormalities. Clin Exp Immunol. 2008;151: 42–50. doi:10.1111/j.1365-2249.2007.03545.x

81. Tarallo P, Henny J, Gueguen R, Siest G. Reference limits of plasma fibrinogen. Eur J Clin Chem Clin Biochem. 1992;30: 745–751.

82. Denko CW, Gabriel P. Age and sex related levels of albumin, ceruloplasmin, alpha 1 antitrypsin, alpha 1 acid glycoprotein, and transferrin. Ann Clin Lab Sci. 1981;11: 63–68.

83. Ritchie RF, Palomaki GE, Neveux LM, Navolotskaia O, Ledue TB, Craig WY. Reference Distributions for Complement Proteins C3 and C4: A Practical, Simple and Clinically Relevant Approach in a Large Cohort. J Clin Lab Anal. 2004;18: 1–8. doi:10.1002/jcla.10100

84. Wahl PW, Warnick GR, Albers JJ, Hoover JJ, Walden CE, Bergelin RO, et al. Distribution of lipoprotein triglyceride and lipoprotein cholesterol in an adult population by age, sex, and hormone use. The pacific northwest bell telephone company health survey. Atherosclerosis. 1981;39: 111–124. doi:10.1016/0021-9150(81)90093-9

85. Shahabi P, Siest G, Herbeth B, Ndiaye NC, Visvikis-Siest S. Clinical necessity of partitioning of human plasma haptoglobin reference intervals by recently-discovered rs2000999. Clin Chim Acta. Elsevier B.V.; 2012;413: 1618–1624. doi:10.1016/j.cca.2012.04.033

86. Yilmaz A, Ulak FŞ, Batun MS. Proton T1 and T2 relaxivities of serum proteins. Magn Reson Imaging. 2004;22: 683–688. doi:10.1016/j.mri.2004.02.001

87. Zacharski L, Ornstein D, Woloshin S, Schwartz L. Association of age, sex, and race with body iron stores in adults: analysis of NHANES III data. Assoc age, sex, race with body iron stores adults Anal NHANES III data. 2000;140: 98–104. doi:10.1067/mhj.2000.106646

88. Kasper CB, Deutsch HF, Beinert H. Studies on the state of copper in native and modified human ceruloplasmin. J Biol Chem. 1963;238: 2338–2342.

89. Nordin BEC, Need a. G, Morris H a., Horowitz M. Biochemical variables in pre- and postmenopausal women: Reconciling the calcium and estrogen hypotheses. Osteoporos Int. 1999;9: 351–357. doi:10.1007/s001980050158

90. Klæstrup E, Trydal T, Pedersen JF, Larsen JM, Lundbye-Christensen S, Kristensen SR. Reference intervals and age and gender dependency for arterial blood gases and electrolytes in adults. Clin Chem Lab Med. 2011;49: 1495–500. doi:10.1515/CCLM.2011.603

91. Yoo KD, Kang S, Choi Y, Yang SH, Heo NJ, Chin HJ, et al. Sex, Age, and the Association of Serum Phosphorus With All-Cause Mortality in Adults With Normal Kidney Function. Am J Kidney Dis. Elsevier Inc; 2016;67: 79–88. doi:10.1053/j.ajkd.2015.06.027

92. Morgan AR, Parker GJM, Roberts C, Buonaccorsi GA, Maguire NC, Hubbard Cristinacce PL, et al. Feasibility assessment of using oxygen-enhanced magnetic resonance imaging for evaluating the effect of pharmacological treatment in COPD. Eur J Radiol. 2014;83: 2093–101. doi:10.1016/j.ejrad.2014.08.004

93. Dietrich O, Gaass T, Reiser MF. T1 relaxation time constants, influence of oxygen, and the oxygen transfer function of the human lung at 1.5 T—A meta-analysis. Eur J Radiol. Elsevier Ireland Ltd; 2017;86: 252–260. doi:10.1016/j.ejrad.2016.11.027

94. Zhang W-J, Niven RM, Young SS, Liu Y-Z, Parker GJM, Naish JH. Dynamic oxygen-enhanced magnetic resonance imaging of the lung in asthma—Initial experience. Eur J Radiol. Elsevier Ireland Ltd; 2015;84: 318–326. doi:10.1016/j.ejrad.2014.10.021

95. Bertini I, Luchinat C, Parigi G, Ravera E. NMR of Paramagnetic Molecules. 2nd Editio. NMR of Parmagnetic Molecules (Second Edition), Applications to Metallobiomolecules and Models. Elsevier Science; 2016. doi:10.1016/B978-0-444-63436-8/00004-1

96. Bloembergen N, Morgan LO. Proton relaxation times in paramagnetic solutions. Effects of electron spin relaxation. J Chem Phys. 1961;34: 842–850. doi:10.1063/1.1731684

97. Teng C-L, Hong H, Kiihne S, Bryant RG. Molecular oxygen spin-lattice relaxation in solutions measured by proton magnetic relaxation dispersion. J Magn Reson. Academic Press; 2001;148: 31–34. doi:10.1006/JMRE.2000.2219

98. Solomon I. Relaxation Processes in a System of Two Spins. Phys Rev. American Physical Society; 1955;99: 559–565. doi:10.1103/PhysRev.99.559

99. Graf V, Noack F, Béné GJ. Proton spin T1relaxation dispersion in liquid H2O by slow proton-exchange. J Chem Phys. 1980;72: 861–863. doi:10.1063/1.439240

100. Berliner LJ, Reuben J. Biological Magnetic Resonance 12: NMR of Parmagnetic Molecules. New York: Plenum Press; 1993.

101. Sendroy J, Dillon RT, Van Slyke DD. Studies of gas and Electrolyte equilibria in Blood, XIX. The solubility and physical state of uncombined oxygen in blood. J Biol Chem. 1934;105: 597–632.

102. Noordin S, Winalski CS, Shortkroff S, Mulkern R V. Factors affecting paramagnetic contrast enhancement in synovial fluid: effects of electrolytes, protein concentrations, and temperature on water proton relaxivities from Mn ions and Gd chelated contrast agents. Osteoarthr Cartil. Elsevier Ltd; 2010;18: 964–970. doi:10.1016/j.joca.2010.03.010

103. Laurens E, Schneider E, Winalski CS, Calabro A. A synthetic cartilage extracellular matrix model: hyaluronan and collagen hydrogel relaxivity, impact of macromolecular concentration on dGEMRIC. Skeletal Radiol. 2012;41: 209–17. doi:10.1007/s00256-011-1331-z

104. Teng CL, Bryant RG. Mapping Oxygen Accessibility to Ribonuclease A Using High-Resolution NMR Relaxation Spectroscopy. Biophys J. Elsevier; 2004;86: 1713–1725. doi:10.1016/S0006-3495(04)74240-X

105. Hueckel P, Schreiber W, Markstaller K, Bellemann M, Kauczor H-U, Thelen M. Effect of Partial Oxygen Pressure and Hematocrit on T1 Relaxation in Human Blood. Proceedings of the International Society for Magnetic Resonance in Medicine. 2000. p. 1586.

106. Kingsley PB. Signal Intensities andT1 Calculations in Multiple-Echo Sequences with Imperfect Pulses. Concepts Magn Reson. Wiley-Blackwell; 1999;11: 29–49. doi:10.1002/(SICI)1099-0534(1999)11:1<29::AID-CMR2>3.0.CO;2-M

107. Siversson C. Three-dimensional T1 quantification techniques for assessment of cartilage quality using dGEMRIC [Internet]. Lund University. 2011. doi:978-91-86871-24-6

108. Takenaka D, Puderbach M, Ohno Y, Risse F, Ley S, Sugimura K, et al. Oxygen-enhanced lung magnetic resonance imaging: influence of inversion pulse slice selectivity on inversion recovery half-Fourier single-shot turbo spin-echo signal. Jpn J Radiol. 2011;29: 244–50. doi:10.1007/s11604-010-0548-4

109. Look DC. Time Saving in Measurement of NMR and EPR Relaxation Times. Rev Sci Instrum. 1970;41: 250. doi:10.1063/1.1684482

110. Brix G, Schad LR, Deimling M, Lorenz WJ. Fast and precise T1 imaging using a TOMROP sequence. Magn Reson Imaging. 1990;8: 351–356. doi:10.1016/0730-725X(90)90041-Y

111. Jakob PM, Hillenbrand CM, Wang T, Schultz G, Hahn D, Haase A. Rapid Quantitative Lung 1 H T 1 Mapping. J Magn Reson imaging. 2001;14: 795–799. doi:10.1002/jmri.10024

112. Deichmann R, Haase A, Hubland A. Quantification of Tl Values by SNAPSHOT-FLASH NMR Imaging. J Magn Reson. 1992;96: 608–612.

113. Wang T, Schultz G, Hebestreit H, Hebestreit A, Hahn D, Jakob PM. Quantitative perfusion mapping of the human lung using 1H spin labeling. J Magn Reson Imaging. 2003;18: 260–5. doi:10.1002/jmri.10338

114. Mai VM, Liu B, Polzin JA, Li W, Kurucay S, Bankier AA, et al. Ventilation-perfusion ratio of signal intensity in human lung using oxygen-enhanced and arterial spin labeling techniques. Magn Reson Med. 2002;48: 341–350. doi:10.1002/mrm.10230

115. Stock KW, Chen Q, Morrin M, Hatabu H, Edelman RR. Oxygen-enhanced magnetic resonance ventilation imaging of the human lung at 0.2 and 1.5 T. J Magn Reson Imaging. 1999;9: 838–841. doi:10.1002/(SICI)1522-2586(199906)9:6<838::AID-JMRI11>3.0.CO;2-H

116. Zavorsky GS, Walley KR, Russell J a. Red cell pulmonary transit times through the healthy human lung. Exp Physiol. 2006;

117. Tibiletti M, Bianchi A, Stiller D, Rasche V. Pulmonary perfusion quantification with flow-sensitive inversion recovery (FAIR) UTE MRI in small animal imaging. NMR Biomed. 2016; 1–9. doi:10.1002/nbm.3657

118. Triphan SMF, Jobst BJ, Flechsig P, Breuer FA, Jakob PM, Biederer J. Oxygen-dependence of T1 in lung tissue as observed in isolated, ventilated porcine lung phantoms. Proceedings of the International Society for Magnetic Resonance in Medicine 22. 2014. p. 2311.

119. Triphan SMF, Jobst BJ, Breuer FA, Wielpütz MO, Kauczor H-U, Biederer J, et al. Echo time dependence of observed T 1 in the human lung. J Magn Reson Imaging. 2015;42: 610–616. doi:10.1002/jmri.24840

120. Lee J-S, Skalak TC. Microvascular Mechanics : Hemodynamics of Systemic and Pulmonary Microcirculation. Springer New York; 1989.

121. Stadler A, Jakob PM, Griswold M, Barth M, Bankier A a. T1 mapping of the entire lung parenchyma: Influence of the respiratory phase in healthy individuals. J Magn Reson Imaging. 2005;21: 759–64. doi:10.1002/jmri.20319

122. Brudin LH, Rhodes CG, Valind SO, Wollmer P, Hughes JMB. Regional lung density and blood volume in nonsmoking and smoking subjects measured by PET. J Appl Physiol. 1987;63: 1324–1334. doi:10.1152/jappl.1987.63.4.1324

123. Kindvall SSI, Diaz S, Svensson J, Wollmer P, Slusarczyk D, Olsson LE. Influence of age and sex on the longitudinal relaxation time, T1, of the lung in healthy never-smokers. J Magn Reson Imaging. 2016;43: 1250–1257. doi:10.1002/jmri.25085

124. Meinel FG, Graef A, Sommer WH, Thierfelder KM, Reiser MF, Johnson TRC. Influence of vascular enhancement, age and gender on pulmonary perfused blood volume quantified by dual-energy-CTPA. Eur J Radiol. Elsevier Ireland Ltd; 2013;82: 1565–1570. doi:10.1016/j.ejrad.2013.04.019

125. Alamidi FD, Morgan AR, Hubbard Cristinacce PL, Nordenmark LH, Hockings PD, Lagerstrand KM, et al. COPD Patients Have Short Lung Magnetic Resonance T 1 Relaxation Time. COPD J Chronic Obstr Pulm Dis. 2015;2555: 1–7. doi:10.3109/15412555.2015.1048851

126. Triphan SMF, Jobst BJ, Anjorin A, Sedlaczek O, Wolf U, Terekhov M, et al. Reproducibility and comparison of oxygenenhanced T1 quantification in COPD and asthma patients. PLoS One. 2017;12: 1–10. doi:10.1371/journal.pone.0172479

127. Jobst BJ, Triphan SMF, Sedlaczek O, Anjorin A, Kauczor HU, Biederer J, et al. Functional lung MRI in chronic obstructive pulmonary disease: comparison of t1 mapping, oxygen-enhanced t1 mapping and dynamic contrast enhanced perfusion. PLoS One. Public Library of Science; 2015;10: e0121520. doi:10.1371/journal.pone.0121520

128. Jakob PM, Wang T, Schultz G, Hebestreit H, Hebestreit A, Hahn D. Assessment of human pulmonary function using oxygen-enhanced T(1) imaging in patients with cystic fibrosis. Magn Reson Med. 2004;51: 1009–16. doi:10.1002/mrm.20051

129. Kindvall S, Alkner S, Kjellén E, Nilsson P, Svensson J, Diaz S, et al. T1-mapping and OE-MRI of patients treated with radiotherapy for breast cancer [Internet]. 2015. Available: http://portal.research.lu.se/portal/sv/publications/t1mapping-and-oemri-of-patients-treated-with-radiotherapy-for-breast-cancer(ecbc3643-c6e9-4288-8074-ea886aa7e141).html

130. Stadler A, Jakob PM, Griswold M, Stiebellehner L, Barth M, Bankier A a. T1 mapping of the entire lung parenchyma: Influence of respiratory phase and correlation to lung function test results in patients with diffuse lung disease. Magn Reson Med. 2008;59: 96–101. doi:10.1002/mrm.21446

131. Erven K, Weltens C, Nackaerts K, Fieuws S, Decramer M, Lievens Y. Changes in pulmonary function up to 10 years after locoregional breast irradiation. Int J Radiat Oncol Biol Phys. 2012;82: 701–707. doi:10.1016/j.ijrobp.2010.12.058

132. Jaén J, Vázquez G, Alonso E, León A, Guerrero R, Almansa JF. Changes in pulmonary function after incidental lung irradiation for breast cancer: A prospective study. Int J Radiat Oncol Biol Phys. 2006;65: 1381–1388. doi:10.1016/j.ijrobp.2006.03.008

133. Renne J, Lauermann P, Hinrichs JB, Schönfeld C, Sorrentino S, Gutberlet M, et al. Chronic Lung Allograft Dysfunction: Oxygen-enhanced T1-Mapping MR Imaging of the Lung. Radiology. Radiological Society of North America Inc.; 2015;276: 266–73. doi:10.1148/radiol.15141486

134. Alamidi DF, Kindvall SSI, Hubbard Cristinacce PL, McGrath DM, Young SS, Naish JH, et al. T1 Relaxation Time in Lungs of Asymptomatic Smokers. PLoS One. 2016;11: e0149760. doi:10.1371/journal.pone.0149760

135. Bosisio E, Grisetti GC, Panzuti F, Sergi M. Pulmonary Diffusing Capacity and Its Components (DM and Vc) in Young, Healthy Smokers. Respiration. 1980;40: 307–310. doi:10.1159/000194297

136. Sansores RH, Pare PD, Abboud RT. Acute Effect of Cigarette Smoking on the Carbon Monoxide Diffusing Capacity of the Lung. Am Rev Respir Dis. 1992;146: 951–958. doi:10.1164/ajrccm/146.4.951

137. Philo JS, Dreyer U, Schuster TM. Diamagnetism of human apo-, oxy-, and (carbonmonoxy)hemoglobin. Biochemistry. 1984;23: 865–72. Available: http://www.ncbi.nlm.nih.gov/pubmed/6712929

138.   Taylor CR, Sostman HD, Gore JC, Smith GW. Proton relaxation times in bleomycin-induced lung injury. Invest Radiol. 1987;22: 621–6. Available: http://www.ncbi.nlm.nih.gov/pubmed/2444553

139.   Cutillo AG, Chan PH, Ailion DC, Watanabe S, Albertine KH, Durney CH, et al. Effects of endotoxin lung injury on NMR T2 relaxation. Magn Reson Med. Wiley-Blackwell; 1998;39: 190–197. doi:10.1002/mrm.1910390205

140.   Cutillo AG, Chan PH, Ailion DC, Watanabe S, Rao N V., Hansen CB, et al. Characterization of bleomycin lung injury by nuclear magnetic resonance: Correlation between NMR relaxation times and lung water and collagen content. Magn Reson Med. 2002;47: 246–256. doi:10.1002/mrm.10082

141.   Jobse BN, McCurry CA, Morissette MC, Rhem RG, Stämpfli MR, Labiris NR. Impact of inflammation, emphysema, and smoking cessation on V/Q in mouse models of lung obstruction. Respir Res. BioMed Central; 2014;15: 42. doi:10.1186/1465-9921-15-42

142.   Easley RB, Fuld MK, Fernandez-Bustamante A, Hoffman EA, Simon BA. Mechanism of Hypoxemia in Acute Lung Injury Evaluated by Multidetector-Row CT. Acad Radiol. 2006;13: 916–921. doi:10.1016/j.acra.2006.02.055

143.   Pearson M. Is the primary mechanism underlying COPD: Inflammation or ischaemia? COPD J Chronic Obstr Pulm Dis. 2013;10: 536–541. doi:10.3109/15412555.2013.763781

144.   Wright JL, Levy RD, Churg A. Pulmonary hypertension in chronic obstructive pulmonary disease: Current theories of pathogenesis and their implications for treatment. Thorax. 2005;60: 605–609. doi:10.1136/thx.2005.042994

145.   Wang DX, Jin XR, Wang WH, Chen G, Du YP, Zhu ZH. Effect of cigarette smoking on hypoxic pulmonary vasoconstriction and its relation to animal species and period of smoking. J Tongji Med Univ. 1992;12: 75–9. Available: http://www.ncbi.nlm.nih.gov/pubmed/1433421

146.   Chen G, Wang DX. Effects of cigarette smoking on hemodynamics and hypoxic pulmonary vasoconstriction: role of prostaglandins and leukotrienes. J Tongji Med Univ. 1989;9: 222–7. Available: http://www.ncbi.nlm.nih.gov/pubmed/2630650

147.   Maron MB, Rickaby DA, Dawson CA. Adrenal component to pulmonary hypertension caused by nicotine administration in the dog. J Appl Physiol. 1980;49: 66–72. doi:10.1152/jappl.1980.49.1.66

148.   Sussan TE, Gajghate S, Thimmulappa RK, Ma J, Kim J-H, Sudini K, et al. Exposure to Electronic Cigarettes Impairs Pulmonary Anti-Bacterial and Anti-Viral Defenses in a Mouse Model. Metzger DW, editor. PLoS One. Public Library of Science; 2015;10: e0116861. doi:10.1371/journal.pone.0116861

149.   Xu Y, Cardell L-O. Long-term nicotine exposure dampens LPS-induced nerve-mediated airway hyperreactivity in murine airways. Am J Physiol Cell Mol Physiol. American Physiological Society Bethesda, MD; 2017;313: L516–L523. doi:10.1152/ajplung.00222.2016

150.   Pinheiro NM, Miranda CJCP, Perini A, Câmara NOS, Costa SKP, Alonso-Vale MIC, et al. Pulmonary inflammation is regulated by the levels of the vesicular acetylcholine transporter. PLoS One. 2015;10. doi:10.1371/journal.pone.0120441

151.   Tripathi A, Bydder GM, Hughes JM, Pennock JM, Goatcher A, Orr JS, et al. Effect of oxygen tension on NMR spin-lattice relaxation rate of blood in vivo. Invest Radiol. 1984;19: 174–8. Available: http://www.ncbi.nlm.nih.gov/pubmed/6469521

152.   Whalen RE, Saltzman HA, Holloway DH, McIntosh HD, Sieker HO, Brown IW, et al. Cardiovascular and blood gas responses to hyperbaric oxygenation. Am J Cardiol. 1965;15: 638–646. Available: http://www.scopus.com/inward/record.url?eid=2-s2.0-0001129257&partnerID=tZOtx3y1

153.   Molinari F, Puderbach M, Eichinger M, Ley S, Fink C, Bonomo L, et al. Oxygen-enhanced magnetic resonance imaging: influence of different gas delivery methods on the T1-changes of the lungs. Invest Radiol. 2008;43: 427–32. doi:10.1097/RLI.0b013e318169012d

154.   Renne J, Lauermann P, Hinrichs J, Schönfeld C, Sorrentino S, Gutberlet M, et al. Clinical use of oxygen-enhanced T1 mapping MRI of the lung: Reproducibility and impact of closed versus loose fit oxygen delivery system. J Magn Reson Imaging. 2013;00: 1–7. doi:10.1002/jmri.24535

155.   Ohno Y, Hatabu H, Takenaka D, Adachi S, Van Cauteren M, Sugimura K. Oxygen-enhanced MR ventilation imaging of the lung: Preliminary clinical experience in 25 subjects. Am J Roentgenol. 2001;177: 185–194. Available: http://www.scopus.com/inward/record.url?eid=2-s2.0-0034989938&partnerID=tZOtx3y1

156.   Ohno Y, Koyama H, Nogami M, Takenaka D, Matsumoto S, Obara M, et al. Dynamic oxygen-enhanced MRI versus quantitative CT: pulmonary functional loss assessment and clinical stage classification of smoking-related COPD. AJR Am J Roentgenol. American Roentgen Ray Society; 2008;190: 8–10. doi:10.2214/AJR.07.2511

157.   Guhan AR, Cooper S, Oborne J, Lewis S, Bennett J, Tattersfield AE. Systemic effects of formoterol and salmeterol : a dose-response comparison in healthy subjects. 2000; 650–656.

158.   Zha W, Kruger SJ, Johnson KM, Cadman R V., Bell LC, Liu F, et al. Pulmonary ventilation imaging in asthma and cystic fibrosis using oxygen-enhanced 3D radial ultrashort echo time MRI. J Magn Reson Imaging. 2017; 1–11. doi:10.1002/jmri.25877

159. Ohno Y, Koyama H, Matsumoto K, Onishi Y, Nogami M, Takenaka D, et al. Oxygen-enhanced MRI vs. quantitatively assessed thin-section CT: pulmonary functional loss assessment and clinical stage classification of asthmatics. Eur J Radiol. Elsevier Ireland Ltd; 2011;77: 85–91. doi:10.1016/j.ejrad.2009.06.027

160. Renne J, Hinrichs J, Schönfeld C, Gutberlet M, Winkler C, Faulenbach C, et al. Noninvasive Quantification of Airway Inflammation Following Segmental Allergen Challenge with Functional MR Imaging: A Proof of Concept Study. Radiology. 2015;274: 267–275. doi:10.1148/radiol.14132607

161. Ohno Y, Nishio M, Koyama H, Yoshikawa T, Matsumoto S, Seki S, et al. Oxygen-enhanced MRI for patients with connective tissue diseases: comparison with thin-section CT of capability for pulmonary functional and disease severity assessment. Eur J Radiol. Elsevier Ireland Ltd; 2014;83: 391–7. doi:10.1016/j.ejrad.2013.11.001

162. Vande Velde G V, De Langhe E, Poelmans J, Dresselaers T, Lories RJ, Himmelreich U. Magnetic Resonance Imaging for Noninvasive Assessment of Lung Fibrosis Onset and Progression: Cross-Validation and Comparison of Different Magnetic Resonance Imaging Protocols With Micro-Computed Tomography and Histology in the Bleomycin-Induced Mouse Mod. Invest Radiol. 2014;49: 691–698. doi:10.1097/RLI.0000000000000071

163. Burris NS, Johnson KM, Larson PEZ, Hope MD, Nagle SK, Behr SC, et al. Detection of Small Pulmonary Nodules with Ultrashort Echo Time Sequences in Oncology Patients by Using a PET/MR System. Radiology. 2015;278: 150489. doi:10.1148/radiol.2015150489

164. Ohno Y, Koyama H, Yoshikawa T, Seki S, Takenaka D, Yui M, et al. Pulmonary high-resolution ultrashort TE MR imaging: Comparison with thin-section standard- and low-dose computed tomography for the assessment of pulmonary parenchyma diseases. J Magn Reson Imaging. 2016;43: 512–532. doi:10.1002/jmri.25008

165. Dournes G, Menut F, Macey J, Fayon M, Chateil J, Salel M, et al. Lung morphology assessment of cystic fibrosis using MRI with ultra-short echo time at submillimeter spatial resolution. 2016; doi:10.1007/s00330-016-4218-5

166. Bianchi A, Tibiletti M, Kjørstad Å, Birk G, Schad LR, Stierstorfer B, et al. Three-dimensional accurate detection of lung emphysema in rats using ultra-short and zero echo time MRI. NMR Biomed. 2015;28: 1471–1479. doi:10.1002/nbm.3417

167. Ma W, Sheikh K, Svenningsen S, Pike D, Guo F, Etemad-rezai R, et al. Ultra-short Echo-Time Pulmonary MRI : Evaluation and Reproducibility in COPD Subjects With and Without Bronchiectasis. 2015;1474: 1465–1474. doi:10.1002/jmri.24680

168. Muller NL, Staples CA, Miller RR, Abboud RT. "Density mask". An objective method to quantitate emphysema using computed tomography. Chest. 1988;94: 782–787. doi:10.1378/chest.94.4.782

169. Zhang WJ, Hubbard Cristinacce PL, Bondesson E, Nordenmark LH, Young SS, Liu YZ, et al. MR Quantitative Equilibrium Signal Mapping: A Reliable Alternative to CT in the Assessment of Emphysema in Patients with Chronic Obstructive Pulmonary Disease. Radiology. 2015;275: 579–588. doi:10.1148/radiol.14132953

170. Burrell JS, Walker-Samuel S, Baker LCJ, Boult JKR, Jamin Y, Halliday J, et al. Exploring dR2* and dR1 as imaging biomarkers of tumor oxygenation. J Magn Reson Imaging. 2013;38: 429–434. doi:10.1002/jmri.23987

171. Lederlin M, Bauman G, Eichinger M, Dinkel J, Brault M, Biederer J, et al. Functional MRI using Fourier decomposition of lung signal: Reproducibility of ventilation- and perfusion-weighted imaging in healthy volunteers. Eur J Radiol. 2013;82: 1015–1022. doi:10.1016/j.ejrad.2012.12.003

172. Bauman G, Scholz A, Rivoire J, Terekhov M, Friedrich J, de Oliveira A, et al. Lung ventilation- and perfusion-weighted Fourier decomposition magnetic resonance imaging: In vivo validation with hyperpolarized ^{3}He and dynamic contrast-enhanced MRI. Magn Reson Med. Wiley-Blackwell; 2013;69: 229–237. doi:10.1002/mrm.24236

173. Kanski M, Arheden H, Wuttge DM, Bozovic G, Hesselstrand R, Ugander M. Pulmonary blood volume indexed to lung volume is reduced in newly diagnosed systemic sclerosis compared to normals--a prospective clinical cardiovascular magnetic resonance study addressing pulmonary vascular changes. J Cardiovasc Magn Reson. 2013;15: 86. doi:10.1186/1532-429X-15-86

174. Su X, Matthay MA, Malik AB. Requisite Role of the Cholinergic α7 Nicotinic Acetylcholine Receptor Pathway in Suppressing Gram-Negative Sepsis-Induced Acute Lung Inflammatory Injury. J Immunol. 2010;184: 401–410. doi:10.4049/jimmunol.0901808

175. Su X, Lee JW, Matthay ZA, Mednick G, Uchida T, Fang X, et al. Activation of the α7 nAChR Reduces Acid-Induced Acute Lung Injury in Mice and Rats. Am J Respir Cell Mol Biol. 2007;37: 186–192. doi:10.1165/rcmb.2006-0240OC

Acknowledgement

Först och främst förlåt till min lillasyster. Jag är ledsen att göra dig besviken, men det blev inget Nobelpris innan jag fyllde 30, däremot gott och väl en doktorsavhandling. Att göra min familj stolt har alltid varit en stark dragkraft när det gått tungt och den här boken är tillägnad er. Ni säger att ni skulle älska mig även om jag hoppade av doktorandstudierna, flyttade hem till landet och inte gjorde annat än att klappa katterna om dagarna – och jag tror er – det ger mig en oerhörd kraft.

Avhandlingen ni har framför er är ju slutet på en lång resa, men allt började redan 2007. Därför måste jag tacka mina fantastiska fysikervänner som höll humöret högt på Rydbergs legendariska källare. Extra tack till Benson och Malin som inte bara är förebilder i forskning, utan verkligen varit viktiga vänner för mig.

Under perioder har jag forskat, grävt i litteratur, scannat försökspersoner och skrivit utkast på artiklar, bara för att hitta ett räknefel i min kod efter månaders arbete. När något sådant hänt har jag sökt sinnesro i körsången. Mitt hår hade för länge sedan grånat om det inte vore för Ostrochorus och Svanholm Singers.

Redan 2011 gjorde jag praktik och examensarbete på Medicinsk strålningsfysik i Malmö. Förutom att Christian lärde mig olympisk tyngdlyftning under denna period, lyfte den varma och öppna stämningen i Malmö en tyngd från mina axlar. Professor Sören Mattson – lika känd för sitt vetenskapliga skarpsinne som sitt rättvisepatos – har säkerligen präglat atmosfären här. Denna levande legend kan inte bara beräkna stråldos från betasönderfall bara av handryggshårens polarisation; han kan också berätta historier, och han vet vikten av att ge alla människor en chans.

En sådan chans gavs till mig av Jonas Svensson, som var min handledare och senare bihandledare. Förtroendet att vikariera för dig var starten på min MR-karriär och du har troget stöttat mig hela vägen.

Här är det dags att tacka LEO, min huvudhandledare och vän. Du klev in i det fönsterlösa arbetsrummet där jag satt med mitt examensarbete och frågade när jag egentligen skulle bli klar med rapporten och börja jobba på riktigt. Efter bara 5 minuter hade du ritat upp en tidslinje med tydligt slut, och därmed sett till att jag fick min legitimation i tid för en löneförhöjning på mitt vikariat. Jag har aldrig förstått om din planeringsförmåga kommer naturligt eller inte, huvudsaken är att du kan tillämpa den på ditt eget och andras arbete. Som handledare balanserar du målsättningar med lösa tyglar och uppmuntrar alltid mina egna vilda idéer. Dessutom vet jag att du anstränger dig för att utvecklas i rollen som både chef och handledare, vilket varit en stor inspiration för mig själv att utvecklas. Tyvärr är denna avhandling inte dedikerad till dig, den är till min familj, däremot får du detta: Ett hjärtligt och tusenfalt tack.

Pulmonary imaging with quantification of T_1-relaxation and oxygen enhanced MRI

Quantification of the longitudinal relaxation time, T_1, and oxygen enhanced (OE-) MRI are two potential imaging biomarkers for lung disease. This thesis explores the physiological relevance of quantitative T_1 measurements and OE-MRI of the lungs and presents a physiological and physical interpretation of these imaging biomarkers based on measurements in healthy volunteers.

This thesis is the perfect starting point for anyone interested in using OE-MRI and T_1-quantification for longitudinal studies of patients or risk groups, and will hopefully make those measurements worthwhile.

Simon Kindvall was awarded the degree of M.Sc. in Medical Physics in 2012 and studied clinical anatomy, cellular biology and human physiology before writing this thesis.

FACULTY OF MEDICINE

Department of Medical Radiation Physics

Lund University, Faculty of Medicine
Doctoral Dissertation Series 2018:152
ISBN 978-91-7619-721-9
ISSN 1652-8220

LUND UNIVERSITY